Science of Remote Sensing 12 (2025) 100301

Contents lists available at ScienceDirect

Science of Remote Sensing

journal homepage: www.sciencedirect.com/journal/science-of-remote-sensing

Annual national tree canopy cover mapping: A novel workflow with temporal transferability and improved uncertainty quantification

Joshua Heyer [a,*], Karen Schleeweis [b], Bonnie Ruefenacht [a], Ian Housman [a], Yang Zhiqiang [b], Daniel Ryerson [c], Jaclyn Reischmann [c], Kevin Megown [c], M. Seth Bogle [a]

[a] *RedCastle Resources, Inc., Contractor to: USDA Forest Service Field Services and Innovation Center Geospatial Office (FSIC-GO), USA*
[b] *USDA Forest Service Rocky Mountain Research Station, Forest Inventory and Analysis, USA*
[c] *USDA Forest Service Field Services and Innovation Center, Geospatial Office (FSIC-GO), USA*

ARTICLE INFO

Keywords:
Tree canopy cover
Forest dynamics
Optical remote sensing
Forest inventory/monitoring
Google earth engine
Uncertainty quantification
Model temporal transferability

ABSTRACT

In 2023, a new generation of National Land Cover Database (NLCD) Tree Canopy Cover (TCC) data were produced that include annual 30m gridded time-series products for the Conterminous United States (CONUS). These NLCD TCC v2021.4 products have more frequent time steps, inter-annual coherency, lower product release latency, improved accuracy, uncertainty metrics, and documentation over previous versions. Our methodology leveraged Google Earth Engine (GEE) to generate annual time-series composites from Landsat and Sentinel-2 imagery that were used to predict annual pixel-wise TCC. Next, we used a moving window approach with a 5x5 window of equal-area tiles (480 × 480 km) to calibrate 54 random forest models on 2011 Forest Inventory and Analysis (FIA) reference data. Then we used model temporal transfer to apply each 2011 model to the window's center tile, with annual time-series predictors, to predict per pixel annual TCC and standard error (SE). To quantify model uncertainty, we simulated uncertainty for each TCC model to derive an uncertainty metric, Tau (τ), which enables users to incorporate confidence boundaries into environmental and ecological applications using the NLCD TCC v2021.4 data. An independent statistical assessment of the 2011 TCC map, conducted using 16,607 FIA observations, yielded a weighted Root Mean Square Deviation ($RMSD_{W)}$) of 12.8 percent TCC and weighted Mean Absolute Error (MAE_W) of 8.0 percent TCC at the CONUS scale. This paper provides a detailed description of the methodology and example use cases of the NLCD TCC and United States Forest Service Science v2021.4 products, paving the way for robust and repeatable future TCC updates.

1. Introduction

Forest structure is crucial for ecosystem health and stability providing vital services that are key to business and industry sustainability and human-wellbeing (Millennium Ecosystem Assessment (Program), 2005a; Millennium Ecosystem Assessment (Program), 2005b; Díaz et al., 2015). Therefore, tree canopy cover (TCC) data, such as the National Land Cover Database (NLCD), are essential for policy and decisions on sustainable management of natural resources. The TCC data meet a diverse set of user communities' needs ranging from public citizens and institutions to private industry, providing critical support for a wide range of practical applications such as forest health, disturbance dynamics and recovery (Poulos et al., 2021; Berryman and McMahan, 2019; Wickham et al., 2023), wind storm economic loss and risk modeling (Lavelle et al., 2023), bioenergy suitability studies (Guler et al., 2022), fractional snow mapping and surface temperatures to inform wildfire risk and water availability (Rittger et al., 2020; Pestana and Lundquist, 2022), urban energy related costs (McDonald et al., 2020), and improving the precision of forest inventory estimates (Freeman et al., 2024; Lister et al., 2020).

TCC data are continuous data that can change gradually or abruptly through space and time, making it distinct from thematic data classifications like forest cover and land use (Nelson et al., 2020). For example, the U.S. Department of Agriculture (USDA), Forest Service, Forest Inventory and Analysis (FIA) Program, the congressionally mandated and authoritative source for data on the nation's forests, uses a forest definition that specifies at least 10 percent TCC of any size tree or has evidence of at least 10 percent TCC in the past, among other criteria (Oswalt et al., 2019). Internationally, the United Nations Food and Agricultural Organization also defines forest as land with potential

* Corresponding author.
E-mail address: joshua.heyer@usda.gov (J. Heyer).

https://doi.org/10.1016/j.srs.2025.100301
Received 11 July 2025; Received in revised form 25 September 2025; Accepted 30 September 2025
Available online 1 October 2025

canopy cover over 10 percent (Food and Agriculture Organization of the United Nations, 2015). Additional criteria used in forest cover class definitions usually include temporal considerations, land use, tree abundance and arrangement, and sometimes species.

In 2001, recognizing the need for spatially continuous authoritative TCC data, the Multi-Resolution Land Characteristics consortium added TCC to the United States Geological Survey (USGS) National Land Cover Database (NLCD) product suite, which included thematic classification and fractional impervious cover layers (Homer et al., 2004; Wickham et al., 2014). In 2011, the USDA Forest Service began producing the NLCD TCC calibrated with the FIA program's Nationwide Forest Inventory data (a plot-based inventory and monitoring data set and a Federal Geographic Data Asset in the same theme), which the Multi-Resolution Land Characteristics consortium continues to distribute as part of the USGS NLCD product suite (Coulston et al., 2012; Homer et al., 2015). These TCC data provide unique complementary data when combined with other components of the NLCD data suite. For example, the NLCD data suite can provide customers across the nation with annual measures of percent canopy cover over impervious surfaces in developed areas to improve estimates of storm water run-off in hydrologic models (Dowtin et al., 2023). NLCD TCC is the only continuous (0–100 percent) TCC Federal Geographic Data Asset in the Land Use - Land Cover theme, that can adequately support both forest inventory (status) and monitoring (trends) (Sohl et al., 2025).

The ability to regularly monitor Earth's surface through time using freely available, moderate resolution (10–30m) imagery, has fueled a revolution in the production of temporally continuous and coherent data products (Woodcock et al., 2020; Drusch et al., 2012; Wulder et al., 2012; Friedl et al., 2022) at national (White et al., 2017; Zhao et al., 2018; Brown et al., 2020; Boryan et al., 2011) and global scales (Gong et al., 2013; Hansen et al., 2013; Buchhorn et al., 2020; Potapov et al., 2022; Zanaga et al., 2022). Data products produced at large scales require significant computing infrastructure and extensive image pre-processing to increase signal-to-noise ratio with the diverse earth observation data. Recognizing these challenges, the NLCD TCC stakeholders identified three goals: 1) produce temporally coherent annual time-series of TCC, 2) improve TCC efficiency and reproducibility, and 3) improve product accuracy and uncertainty metric reporting.

To meet NLCD stakeholders' goals, we developed an innovative workflow that combines local and Google Earth Engine (GEE) environments with full consideration of decreasing development costs and increasing production speed (Gorelick et al., 2017; Woodcock et al., 2008; Wulder et al., 2022). GEE offers a comprehensive library of imagery assets and derivatives, enabling quick processing using high-performance parallel computing capabilities, which reduces the need for extensive in-house information technology capabilities and subjective manual analyst steps that increase development costs, such as those needed to reduce boundary artifacts (Hansen and Loveland, 2012; Ruefenacht et al., 2022; Yang et al., 2018). The hybrid of cloud and local processing allowed us to release an annual TCC dataset with full accuracy and uncertainty characterization without compromising model performance. GEE computing costs, managed through Google Cloud Platform, were an initial consideration and will continue to be monitored for future NLCD TCC data releases.

This manuscript summarizes how the USDA Forest Service met stakeholders' needs with innovative workflows developed and implemented in local and GEE environments used for image processing, modeling, and post-regression routines, as well as more robust quality assurance, reference data, and accuracy assessments. These new techniques were first incorporated into the USDA Forest Service production of the annual CONUS NLCD TCC v2021.4 that includes the Science (2008–2021) and NLCD (2011–2021) TCC products released publicly in 2023.

2. Methodology

Fig. 1 illustrates the new USDA Forest Service TCC workflow that was developed and rigorously tested over several years to produce the annual NLCD TCC v2021.4 products. The testing and implementation of the new workflow techniques were piloted over at least 4–6 of our GEE processing tiles (each roughly the size of Colorado). We first performed Quality Assurance (QA) and Quality Control (QC) – together referred to as QAQC – on 2011 FIA reference data on local computers and leveraged GEE to generate predictor data that includes static terrain, Cropland Data Layer data, and fitted spectral data. Static and 2011 fitted spectral predictor data were exported for local processing where they were joined with the QAQC 2011 FIA reference data in training tables to calibrate and create time-invariant Random Forest (RF) models. The time-invariant RF models were generated across 54 equal-area tiles (480 × 480 km) using a 5x5 moving window approach that avoided GEE memory constraints and reduced model output artifacts. Next, RF models were ingested into GEE and used to predict annual Science TCC images that include two model outputs: per-pixel TCC predictions and model errors. Following model prediction, we implemented a post-regression routine that was applied to the Science TCC images to produce NLCD TCC. The post-regression routine reduced artifacts and interannual noise, resulting in more stable TCC trends. The workflow developed to produce annual TCC products has multiple outputs including the annual Science TCC and Standard Error (SE), information on model uncertainty (Tau) and model performance, and the refined annual NLCD TCC product (TCC only).

2.1. Reference data

For decades, efficacy and cost criteria for national scope management-level projects have dictated that remotely sensed TCC estimates are the only feasible option for wide-scale data capture. There are many ways to quantify percent TCC – the amount of tree cover for a specific area of observation – each with its own strengths, weaknesses, accuracies, and application suitability (Jennings et al., 1999; Gatziolis, 2012; Ma et al., 2017; Tang et al., 2019; Tompalski et al., 2021; Smith et al., 2008). For the NLCD TCC project, the FIA program photo-interpreted tree (crown) canopy cover on 63,010 plots using the FIA annual inventory probabilistic sample design for the 2011 panel (Ruefenacht et al., 2022; Bechtold and Patterson, 2005). The photointerpretation protocol and associated quality control procedures are documented by Goeking et al. (2012). USDA National Agriculture Imagery Program 1-m 4-band imagery was used, with imagery primarily from 2011 or earlier, depending on each state's National Agriculture Imagery Program acquisition schedule (USDA Farm Production and Conservation).

Data quality is often more important than data quantity in machine learning. To ensure data quality, we implemented proactive preventative QAQC measures to identify and address potential issues with the reference data plots. We removed 476 plots due to quality issues, 1972 plots with low confidence based on FIA data collection protocols, and 703 plots with multiple photo interpretations (Ruefenacht et al., 2022).

To ensure stability of reference data over time, we implemented three temporal QAQC procedures: spectral stability, false zero TCC, and temporal mismatches. For the spectral stability procedure, we normalized the time-series of annual spectral composites (see section 2.2) and identified reference data plots that intersected pixels with low spectral variability through time. We combined these data with predictor data (see section 2.2) creating spectrally stable training datasets. We applied bootstrap and RF algorithms in R to these datasets creating 500 bootstrapped TCC predictions (R Core Team, 2020). We differenced the TCC observed and bootstrapped TCC predicted values through time. We used a threshold of greater than 70 percent difference to flag potential unstable reference data plots. These plots were visually examined by experienced analysts, resulting in the removal of 47 low quality

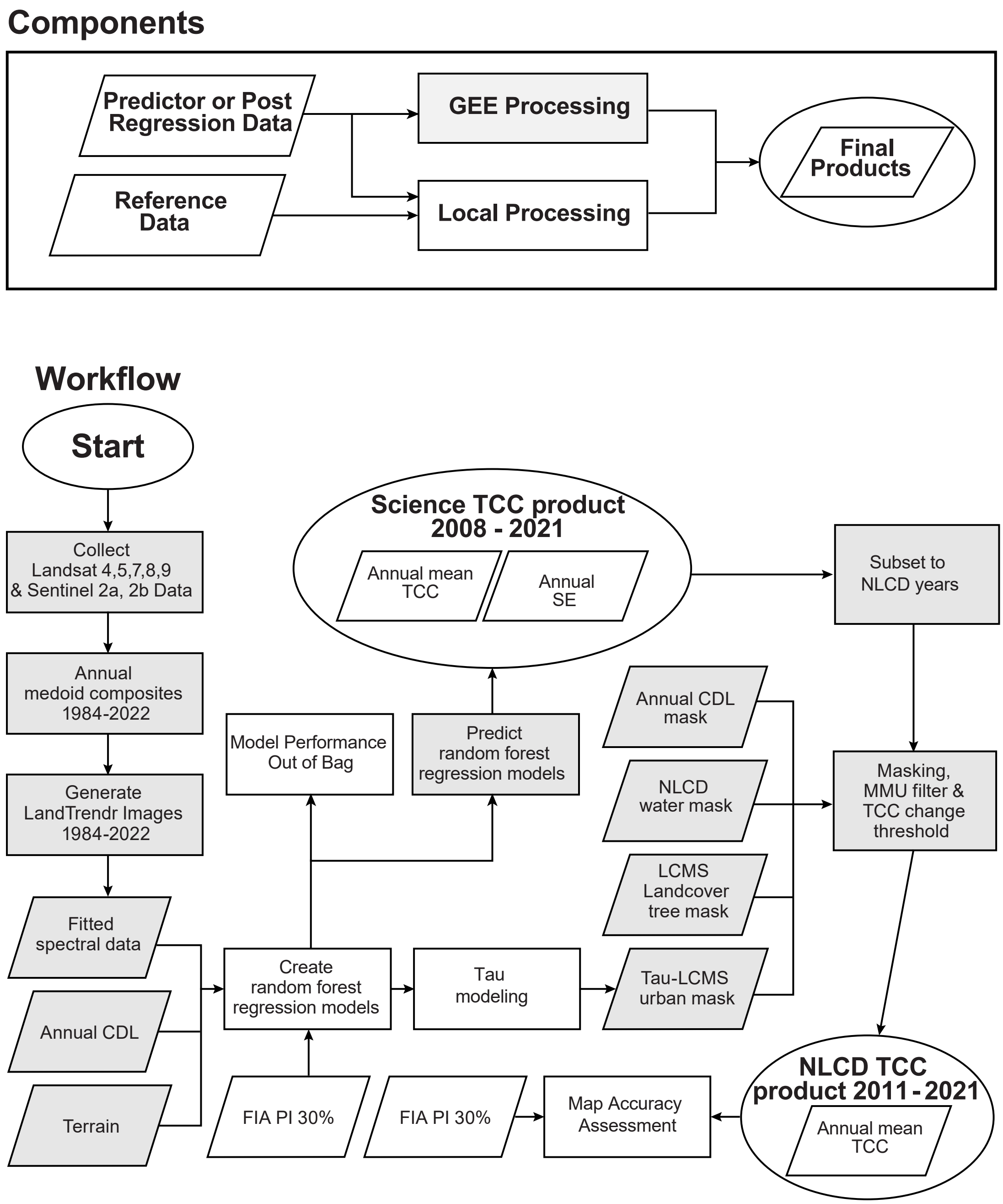

Fig. 1. The NLCD TCC v2021.4 workflow for the Science and NLCD TCC products. The workflow components legend labels characteristics in the larger workflow diagram.

reference data plots.

The second temporal QAQC check was designed to evaluate false zero TCC observations. We identified 844 reference data records with both a TCC value of less than one percent and a tree-covered label in the intersecting pixel of the Forest Service Landscape Change Monitoring System (LCMS) product (USDA Forest Service, 2023). Analysts inspected high resolution aerial imagery at these locations and confirmed 549 reference data plots were true positives (i.e., zero TCC values). The remaining 295 reference data plots were predominantly located in the Southwestern US, where discriminating shrub vs tree cover in 1 m imagery is notoriously challenging. These plots were removed from the reference data.

The final temporal QAQC check was designed to address noise introduced to the modeling relationships due to temporal mismatches. The National Agriculture Imagery Program imagery used in the TCC photointerpretation ranged from 2009 to 2011, while predictor data used for model building is from 2011 (see section 2.2). If reference data locations experienced tree cover losses or gains after the imagery data used for photointerpretation and prior to collection dates for the 2011 spectral predictors, this temporal imprecision could introduce noise to the models. We identified and removed 1384 reference data plots that intersected with LCMS-labeled forest cover loss and 2792 that intersected with LCMS-labeled forest cover gain between 2008 and 2012, mostly in the highly dynamic forest systems of the Southeastern US.

In total, these QAQC efforts removed 7.9 percent of reference data plots from the original dataset. The remaining 55,356 reference data plots were randomly divided into two groups −70 percent for model training and 30 percent for independent map accuracy assessment. Table 1 includes the number of reference data plots used in each 5x5 moving window tile model.

Table 1
Number of plots used for model training, mean observed tree canopy cover with standard deviations, and random forest out-of-bag model performance metrics (root mean square deviation and percent variance explained) for each of the 54 mapping tiles and for each set of predictors.

Tile	Number of Plots	Set 1			Set 2		
		mean tcc ±sd	RMSD	PVE	mean tcc ±sd	RMSD	PVE
0	11,491	26.3 ± 36.4	13.5	86.1	32.8 ± 36.0	13.5	86.2
1	12,103	36.9 ± 40.9	14.3	87.7	37.5 ± 40.6	14.2	87.9
2	9133	50.3 ± 42.8	14.4	88.7	39.4 ± 42.6	14.3	88.7
3	6498	51.6 ± 42.7	14.2	88.9	39.6 ± 42.5	14.2	88.9
4	10,638	9.1 ± 17.0	10.2	63.4	13.2 ± 16.7	10.2	63.6
5	14,773	9.1 ± 17.9	11.3	60.1	13.6 ± 17.9	11.3	60.5
6	18,725	14.5 ± 26.7	12.0	79.7	23.3 ± 26.6	11.9	79.9
7	21,013	19.7 ± 31.8	12.8	83.7	28.3 ± 31.5	12.7	83.9
8	21,828	28.5 ± 37.9	13.5	87.1	34.4 ± 37.6	13.5	87.3
9	21,219	35.1 ± 40.4	14.1	87.8	36.9 ± 40.1	14.0	87.9
10	17.096	41.4 ± 41.5	14.0	88.6	38.4 ± 41.3	13.9	88.7
11	12,607	44.5 ± 41.7	13.9	88.9	38.6 ± 41.5	13.8	89.1
12	10,400	10.3 ± 20.2	10.4	73.2	17.0 ± 20.1	10.4	73.2
13	16,060	9.3 ± 18.9	10.3	70.2	15.6 ± 18.8	10.3	70.5
14	22,078	8.6 ± 18.6	10.9	65.4	14.7 ± 18.6	10.9	65.8
15	28,423	12.0 ± 24.6	11.3	78.9	21.1 ± 24.4	11.2	79.2
16	31,512	17.5 ± 30.3	12.2	83.7	27.1 ± 30.1	12.2	83.8
17	31,475	24.6 ± 35.9	13.0	86.9	32.9 ± 35.7	12.9	87.1
18	30,570	31.8 ± 39.1	13.6	87.8	35.8 ± 38.9	13.5	87.9
19	25,200	38.6 ± 40.4	13.8	88.4	37.3 ± 40.2	13.6	88.6
20	17,856	44.3 ± 40.6	14.1	88.0	37.3 ± 40.4	13.9	88.2
21	10,815	51.7 ± 40.1	14.2	87.4	36.6 ± 39.9	14.0	87.7
22	12,897	13.9 ± 24.8	11.3	79.3	21.9 ± 24.8	11.3	79.4
23	19,939	11.3 ± 22.1	10.6	76.9	19.1 ± 22.1	10.6	77.1
24	26,858	9.8 ± 20.8	10.9	72.8	17.5 ± 20.8	10.8	72.9
25	34,483	12.8 ± 25.5	11.3	80.3	22.2 ± 25.3	11.2	80.6
26	37,158	18.0 ± 30.7	12.2	84.3	27.6 ± 30.5	12.1	84.5
27	35,763	23.8 ± 35.6	12.7	87.3	32.4 ± 35.4	12.6	87.4
28	33,098	31.5 ± 39.0	13.4	88.1	35.7 ± 38.7	13.3	88.3
29	27.503	39.8 ± 40.4	13.8	88.3	37.3 ± 40.2	13.6	88.6
30	18,653	46.8 ± 40.5	13.9	88.1	37.5 ± 40.4	13.8	88.4
31	11,111	54.4 ± 39.4	13.9	87.6	36.1 ± 39.3	13.7	87.9
32	12,627	14.4 ± 25.2	11.4	79.6	22.3 ± 25.3	11.4	79.7
33	18,924	11.7 ± 22.7	10.6	78.5	20.0 ± 22.7	10.5	78.8
34	24,940	9.6 ± 20.8	9.9	77.2	18.1 ± 20.8	9.9	77.5
35	31,432	11.4 ± 23.7	10.4	80.9	20.8 ± 23.6	10.3	81.2
36	33,190	16.2 ± 29.0	11.4	84.6	26.2 ± 29.0	11.3	84.9
37	31,234	21.6 ± 34.2	11.8	88.1	31.5 ± 34.0	11.7	88.3
38	29,010	29.7 ± 38.2	12.6	89.1	35.4 ± 38.0	12.5	89.3
39	24,318	38.4 ± 39.8	13.5	88.4	36.7 ± 39.7	13.4	88.7
40	16,582	46.3 ± 40.2	13.7	88.4	37.1 ± 40.0	13.5	88.6
41	9892	54.9 ± 39.1	13.5	88.1	36.1 ± 39.0	13.3	88.4
42	9997	16.7 ± 27.3	12.2	79.8	24.0 ± 27.3	12.2	80.1
43	14,726	13.1 ± 24.6	11.1	79.8	21.8 ± 24.6	11.0	80.0
44	19,727	10.2 ± 22.1	9.9	79.9	19.6 ± 22.1	9.9	80.0
45	24,820	10.3 ± 22.1	9.6	81.0	19.5 ± 22.1	9.6	81.4
46	26,042	14.3 ± 27.0	10.5	84.8	24.5 ± 26.9	10.5	85.0
47	24,071	17.1 ± 30.4	10.6	87.9	28.0 ± 30.3	10.5	88.0
48	22,616	25.1 ± 35.4	11.5	89.5	33.1 ± 35.4	11.4	89.7
49	18,934	34.3 ± 38.1	12.7	88.9	35.4 ± 38.0	12.5	89.1
50	12,678	43.4 ± 39.1	13.2	88.5	36.2 ± 39.0	13.1	88.7
51	7524	52.2 ± 38.3	13.2	88.2	35.5 ± 38.3	13.0	88.4
52	6221	19.6 ± 30.5	12.4	83.5	27.7 ± 30.6	12.4	83.6
53	9398	14.2 ± 26.8	10.8	84.0	24.5 ± 27.0	10.7	84.2

2.2. Predictor data

We used spectral data from all available Sentinel-2 and Landsat 5–8 imagery within a growing season window to generate annual-medoid composites from 1984 to 2022. On a pixel-wise basis, the medoid is the value that minimizes the sum of square difference between the median value of each band's value to ensure that composite pixel values are taken from a single date across bands (Flood, 2013). Medoid composites were produced from top-of-atmosphere Landsat collection 2 data provided by the USGS and Sentinel-2 provided by the European Space Agency Copernicus Earth observation program, both accessed from the GEE Data Catalog (Landsat Collections in Earth Engine | Earth Engine Data Catalog; Harmonized Sentinel-2 MSI and Instrument). A cross-sensor correction was not warranted based on Chastain et al. (2019), findings of minimal, unbiased top-of-atmosphere reflectance differences between Landsat and Sentinel-2 making further corrections unnecessary for regional and continental scale analyses seeking to maximize temporal frequency and spatial coverage. All spectral data were projected to the Albers Conical Equal Area coordinate system and snapped to the NLCD grid.

The Landsat 7 scan line correction failure in 2003 created unacceptable artifacts in model outputs during workflow pilot test runs. Dropping Landsat 7 imagery all together, however, also created poor outputs in pilot testing, due to image scarcity between 2003 and 2015 leading to a higher number of gaps in the time-series record and resulting in sub-standard spectral composite quality. To solve these issues, and keep the spectral record as stable as possible, we produced two sets of annual-medoid composites (Set 1 and Set 2 predictor data can be found in the Supplementary Table 1). Set1 used all available Sentinel-2 and Landsat 5, 7, and 8 images, excluding all Landsat 7 data after 2002. Set2 used all available Sentinel-2 and Landsat 5, 7, and 8 images, excluding only Landsat 7 bands most affected by scan line correction striping artifacts: the visible, near-infrared bands and associated calculated indices after 2002. In 2016, once Sentinel-2 imagery became available, the five-day repeat acquisition strategy introduced volume processing challenges due to the abundance of available images. We addressed this by shortening the growing season date range window. The growing season window was June 1 to September 30 for composite years prior to 2016 and July 1 to September 1 for composite years 2016 and later.

To eliminate no or bad data pixels caused by clouds, shadows, or other anomalies and to temporally smooth the annual-medoid composites, we used the Landsat-based detection of Trends in Disturbance and Recovery (LandTrendr) algorithm in GEE (Kennedy et al., 2018). LandTrendr iteratively breaks annual-composite time-series into linear segments with fitted spectral values outputting a smoothed time series of spectral images. We ran LandTrendr separately on set1 and set2 composite stacks.

Annual binary agriculture data were derived from the annual national Cropland Data Layer by re-classifying all non-tree crops as agriculture and all remaining classes are non-agriculture (USDA National Agricultural Statistics Service, 2008). Static terrain datasets used include elevation, slope, and aspect from the US National Elevation Dataset produced by the USGS 3D Elevation Program (Geological Survey, 2019; Gesch et al., 2002, 2018). Aspect – cosine and sine – transformations were also used. Annual binary agriculture data and static terrain datasets were stacked with the set1 and set2 LandTrendr time series, to create two model predictor data stacks.

2.3. Modeling

2.3.1. Spatial considerations and testing

It is common practice when modeling over large spatial extents to split reference and predictor data into geographic subpopulations, build spatially explicit RF models, use the models to predict only the area defined by the model training data, and finally, stitch the contiguous predictions together to cover the full extent of interest. This approach is believed to optimize the tradeoffs between (1) storage and processing costs, (2) local variability in calibration and predictor data impact on model performance and fit, (3) post-regression costs to reduce seam-line artifacts at model boundaries, and (4) the ability of reference data density to sufficiently support both model training and independent map validation needs. However, the approach is known to create artifacts, especially evident in model predictions along the seam lines or boundaries (in space and time) between image processing units and model subpopulations units.

The use of irregular shaped ecologically based geographic zones to subset model populations for national extent mapping is common. The Annual NLCD Land Use Land Cover thematic classification models use a step-wise model hierarchy culminating in 20 discrete modeling zones (Geological Survey, 2024). LANDFIRE products, as of 2023, used 13 discrete zones for modeling TCC and height and existing vegetation type maps (La Puma, 2023). The national annual Cropland Data Layer data use 48 state level model zones (Boryan et al., 2011). Commonly used ecozones are built by grouping similar ecosystem characteristics. Therefore, they tend to have discrete boundaries right in transition zones between ecosystems. This presents challenges when using ecozones to subset model populations. The dissimilarity across ecosystem transition zones translates directly into dissimilarities between edges of model transition zones. This can result in egregious boundary effects and potentially poor model predictions in transition zones, which by nature are often of high interest in time-series inventory and monitoring records.

The previous NLCD TCC modeling approach, using the 66 USGS CONUS ecozones (Homer et al., 2004; Ruefenacht et al., 2022), could not support current Forest Service business needs for TCC products. Tipton et al. (2012) found that, when modeling TCC in equally size grid subsets, increasing sample spatial density above the base FIA program intensity (approximately 1 sample per 2428 ha (6000 acres or 24 km^2)) yielded only marginal improvements in model performance across diverse landscapes, provided the absolute number of samples was at least roughly 1500 samples per model. Moisen et al. (2012) found that when calibrated over much larger regions, TCC models could be used to predict smaller subsets with no compromise in model performance. In temporally coherent model calibration and application, it is not uncommon to create temporal subpopulations for model training and calibration using temporal moving windows to subset reference data (e.g. Su et al. (2021)); however, this approach (moving windows to subset reference data) has not been widely applied to spatially coherent model training and application.

We tested multiple approaches to subset geographic model subpopulations: different scales of ecozones (six aggregated USGS zones, CONUS-wide boundaries), equal-area grid at different tile sizes (individual 54 equal-area tiles (480 × 480 km), 3x3 tile aggregate, and 5x5 tile aggregate), and moving windows with different window sizes. Five assessment criteria were used to evaluate results: 1) quantity and arrangement of seam-line artifacts in mapped TCC and Standard Error (SE), 2) visual quality of mapped TCC and SE at local scales, 3) statistical model performance metrics, 4) representative variability between training and predictor data across geographic subpopulations, and 5) ability to hold out 30 percent of reference data for independent map validation that were in line with previous literatures' guides for reference data density.

Different spatial modeling approaches failed different evaluation criteria. Merging USGS zones into six larger units yielded too many and too severe seam lines at model-boundary edges. The CONUS wide approach resulted in a sub-standard map when visually assessed for TCC prediction quality at local scales. We used 54 equal-area tiles (480 × 480 km), where the tile size was dictated by GEE memory and I/O constraints rather than by an autocorrelation test. The 54 equal-area tile approach generated no boundary artifacts between neighboring tiles of mapped outputs, likely due to the tile size being smaller than the limit of spatial autocorrelation in local conditions as captured in the model predictors. However, the approach failed to contain the minimum acceptable density of 1000 reference data plots per model area, for 27 of the 54 tiles (Coulston et al., 2012). Tests using a larger standard tile size (roughly 2*10^6 km or a combination of a 3x3 neighborhood of the 480 × 480 km tiles) failed model-performance metric criteria and the presence of seam-line artifacts.

One approach successfully met all criteria: the moving window approach, where each of the 54 tiles was used as a center tile of a 5x5 tile window (Fig. 2). For each iteration, training data is gathered from the 5x5 tile window, but the resulting model is applied only to the window's center tile. For each year, all 54 tile model outputs are mosaiced together to create one image per year. Local visual inspections of predictions revealed no anomalies or seam lines, and model performance metrics fell within expected range of values. Reference data plot counts for the training datasets ranged from 4311 to 25,993. This abundance of data allowed us to consider the possibility of withholding data for independent map validation assessments. We examined how the frequency and range of TCC values would change when withholding reference data. These examinations showed the frequency and range of TCC values were well represented even when as much as 30 percent of the reference data were withheld.

2.3.2. Temporal considerations and testing

Temporal transferability of models, applied outside of the reference data time period, is not a new concept and cross-temporal validation is documented (Filippelli et al., 2024). Time-invariant models, a subset of temporal transfer, predicts annual time-series of land-cover data for

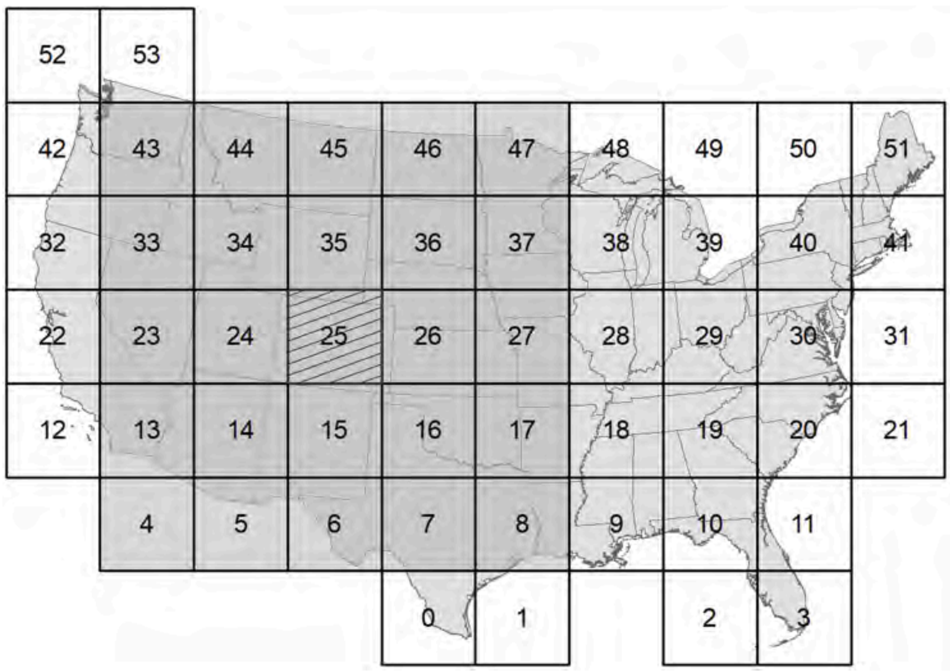

Fig. 2. Illustration of the 54 equal-area tiles (480 × 480 km) used for modeling and mapping TCC in GEE. The training datasets are drawn from 5x5 tile windows. We applied the RF generated predictions to only the center tile. This illustration shows the center.

years of spectral predictors that were not used to train the models (Vogeler et al., 2018). This method presumes a model of the relationships between one year of spectral predictors and reference data can be applied to other years of predictor data resulting in a time-series of predictions that are a function of real changes in the reflectance of the biophysical characteristics of surface vegetation. Sources of noise in the time-series of the predictor data must be low. As recent advances in image processing are constantly improving remote sensing data resources (see section 2.2), noise in the data is being reduced.

We tested the temporal transferability of the RF model outputs over four pilot tiles from distinct ecoregions in the CONUS. Tiles selected included tile 14 in the Southwest CONUS characterized by Pinyon-Juniper and Ponderosa forests, tile 19 in the Southeast characterized by deciduous and conifer forests, tile 38 in the upper-Midwest dominated by deciduous forests, and tile 43 in the Northwest characterized by conifer forests (Fig. 2). Initial testing identified obvious issues due to lack of consistency in the spectral record (see section 2.2). Additional testing evaluated if stable areas in the forest landscape also remained stable in the TCC time-invariant model outputs. These tests indicate whether the time-invariant model approach assumption of reasonable consistency in time-series predictors through time are met.

To test the stability of the time-invariant model outputs, we extracted predictor year 2011 values from both predictor set1 and predictor set2 separately (see section 2.2) for reference data within 5x5 tile windows centered over each pilot tile. We combined these predictor datasets with associated reference data creating two training datasets: one for the set1 predictors and the other for the set2 predictors. We created RF models for both training datasets. We used the RF model built using the set1 predictors to predict pixel-wise TCC and SE for each pilot tile for the years 2016 through 2019. We used the RF model built using the set2 predictors to predict pixel-wise TCC and SE for each pilot tile for the years 2008 through 2015. We defined stable areas in the forested landscape of each pilot tile by first filtering all pixels in each tile using the 2011 NLCD Land Cover forest map classes 41, 42, and 43 (Dewitz and Geological Survey, 2021). Next, we calculated spectral data variability metrics for the NLCD forest pixels through time by normalizing all spectral predictor layers for each year. We averaged the normalized values for each pixel and computed standard deviations for each pixel's time-series of image spectral predictor data. We selected a conservative threshold of <0.0009 standard deviation to identify pixels with temporal stability across the spectral time-series. Finally, we ran a bootstrap analysis on these spectrally stable forest locations to test if the TCC values predicted from the time-invariant modeling approach also remained stable through time.

2.3.3. *National scale modeling, error and uncertainty*

The TCC workflow was accomplished within GEE and on local servers (Fig. 1). GEE's high-performance cloud storage and computing compacity enabled efficient processing of wall-to-wall annual composites and ancillary data, smoothing time-series spectral imagery, rapid application of RF models and post-regression filters, and unparallel exploration and analytical applications support with the geeViz package for quality assessment and other processes (Housman). Robust local servers, ensured we upheld FIA confidentiality responsibilities and protocols during extraction of predictor stack values over reference data locations, training RF models, and modeling prediction uncertainty (Tau) (see section 2.3.4).

Using the 5x5 moving window approach (see section 2.3.1) to subset reference and predictor data, we produced RF models for each 54 equal-area tiles with the Scikit-Learn sklearn.ensemble.RandomForestRegressor function (Breiman, 2001; Pedregosa et al., 2011). To determine the optimal number of variables for each decision tree split (mtry), we employed the tuneRF function within the randomForest package in R (R Core Team, 2020). For the sklearn.ensemble.RandomForestRegressor function, we set the min_samples_leaf to the mtry results and the maxsamples parameter was set to use 63.2 percent of the training data to mirror the out-of-bag (OOB) procedure performed by the R RF algorithm. Scikit-Learn was chosen over R to generate the RF models because it permits the exportation of RF decision trees as text files, which can be imported into GEE to generate TCC maps. To avoid memory errors during model ingestion into GEE, models greater than 15 mb were divided into separate files of 15 mb or less and ingested into GEE as blobs.

GEE allowed us to efficiently apply the time-invariant 2011 TCC models to annual predictor stacks to predict pixel-wise mean TCC and SE for every 30-m pixel across the CONUS for years 2008–2021. In GEE the

RF decision tree blobs were concatenated according to their moving window tile before applying them using the ee.Classifier.decisionTreeEnsemble function with the output mode set to RAW_REGRESSION. The RAW_REGRESSION setting preserves all individual decision tree TCC estimates for each pixel. We set the number of decision trees for the RF algorithm to 500 and averaged the end node TCC estimates. End node TCC variances were also recorded, and SE calculated by taking the square root of the variances on a pixel-wise basis. For map years prior to and including 2015 the TCC Set2 2011 model and corresponding predictors were used to TCC and SE. For map years 2016 and onwards, TCC and SE predictions were generated using the 2011 TCC set1 model and set1 predictor stack.

2.3.4. Modeling Tau uncertainty

Pixel-wise SE from model predictions describes one aspect of uncertainty in image-based predictions, specifically, how much the mean predicted value of the pixel would vary if the model were repeatedly trained and tested on different bootstrap samples. However, a known limitation of RF models is that they cannot extrapolate beyond the range of their initial training data values. Coulston et al. (2016) developed a Tau (τ) statistic to address the need for a more probabilistic (inference enabled) measure of model uncertainty especially for applications where the confidence of the predictions are important, such as environmental and ecological modeling. Tau (τ) provides a measure of uncertainty for new observations. Tau outputs approximation of the prediction uncertainty which can be used to construct confidence intervals around the predictions themselves.

For each of the 54 equal-area RF models, we calculated the Tau (τ) statistic by calculating the standard deviation and RF predictions from individual trees within the ensemble. We simulated data by randomly resampling the training data 2000 times and generating RF models for each of these iterations. Each of these iterations retain the observed and predicted TCC values for the approximate 37 percent holdout datasets allowing comparisons between the variability in the tree-level predictions and the true error. These pairs of observations and predictions were used to calculate Tau (τ) using Equation (1).

$$\tau = \sqrt{\frac{(observed - predicted)^2}{var(predicted)}} \quad \text{Equation 1}$$

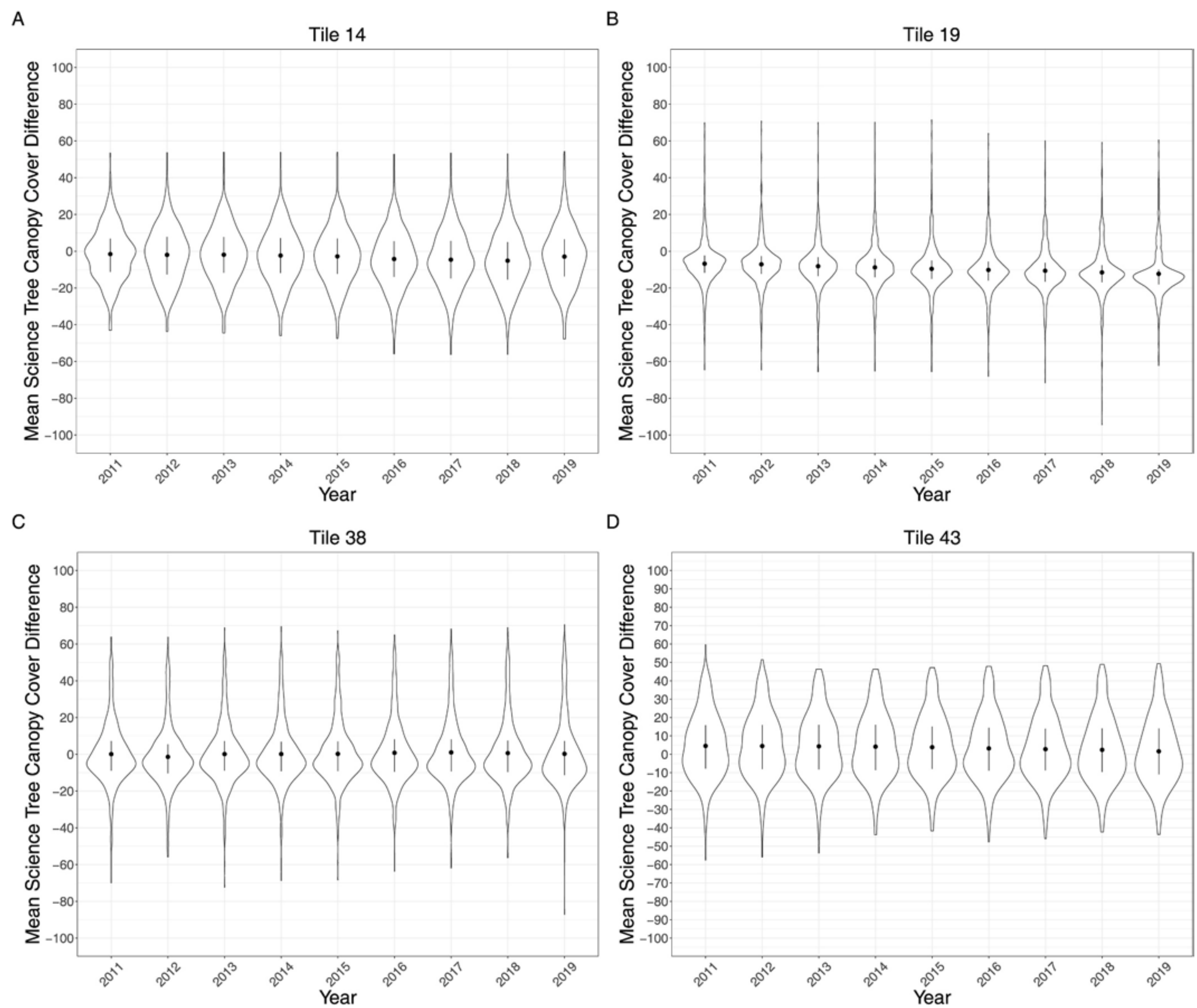

Fig. 3. Mean TCC differences (predicted TCC – observed TCC) for stable pixels through time for four modeling tiles: 14 (275 plots), 19 (928 plots), 38 (541 plots), and 43 (246 plots). The dots and lines in the middle of the violin plots represent the mean diff.

2.4. Post-regression routines

The Multi-Resolution Land Characteristics consortium NLCD products have traditionally served many end users of geospatial data, including policy and land managers. As such they have a high level of cartographic post-regression to bridge the gap between raw spatial data and a consumer ready product, often improving accuracy, reliability, and the maps usability and accessibility across broad audiences. We developed a post-regression workflow to turn the scientific TCC raw-spatial data outputs into the final NLCD TCC v2021.4 maps using a sequence of routines (Fig. 4).

2.4.1. Non-tree masks

TCC values were predicted over all pixels, which results in non-zero TCC values over water, impervious features, and other visible-from-above features where there are no trees. Non-tree masks were applied to Science TCC data to create the NLCD TCC product. We mask non-treed pixels using three masks: a tree mask created from the LCMS Land Cover tree classes (USDA Forest Service, 2023), an agriculture mask created from the annual Crop Data Layer non-tree crops (Boryan et al., 2011; USDA National Agricultural Statistics Service, 2008), and a water mask created from the NLCD water class (Dewitz and Geological Survey, 2021). The LCMS tree mask is the three-year moving window mode of the LCMS Land Cover tree class time-series. We combine the three non-tree masks to recode TCC to zero for pixel's that were flagged non-tree in the non-tree mask.

For non-urban areas, we applied a minimum-mapping unit to mask small clumps of trees. We defined the minimum-mapping unit as tree clumps greater than four connected pixels in size (30 × 30 m*4 or greater), using queen's case of adjacency (nine neighbor). Non-urban tree clumps less than or equal to four connected pixels was recoded to zero percent TCC.

Trees in urban landscapes, where single broad canopy trees exist over impervious surfaces, warrant specific filtering techniques. We first define urban areas using the Topologically Integrated Geographic Encoding and Referencing U.S. Census Block 2018 data (Marx, 1986) and refine the boundaries further using the LCMS Land Use "developed" class, because even within an urban boundary there are "non--developed" areas. At pixels which both Topologically Integrated Geographic Encoding and Referencing data and LCMS Land Use label "developed" urban areas, we masked (set to zero) the TCC pixel values where the magnitude of the TCC value in a pixel is not greater than or equal to the product of its SE and Tau value at the 87th confidence percentile (see section 2.3.4).

2.4.2. Change magnitude thresholds

Fitting routines can be applied on predicted outputs to reduce interannual noise and return longer duration trends (Kennedy et al., 2010). To reduce minor interannual variability in the NLCD TCC time record, we applied a simple per-pixel fitting routine. This routine is applied to the TCC time-series after masking, and updates TCC values when a minimum change threshold is met. First, we established a baseline TCC value (TCC_{baseyr}) for 2011. The TCC_{baseyr} is the median TCC value from 2008 to 2010. For each year following the TCC_{baseyr}, we

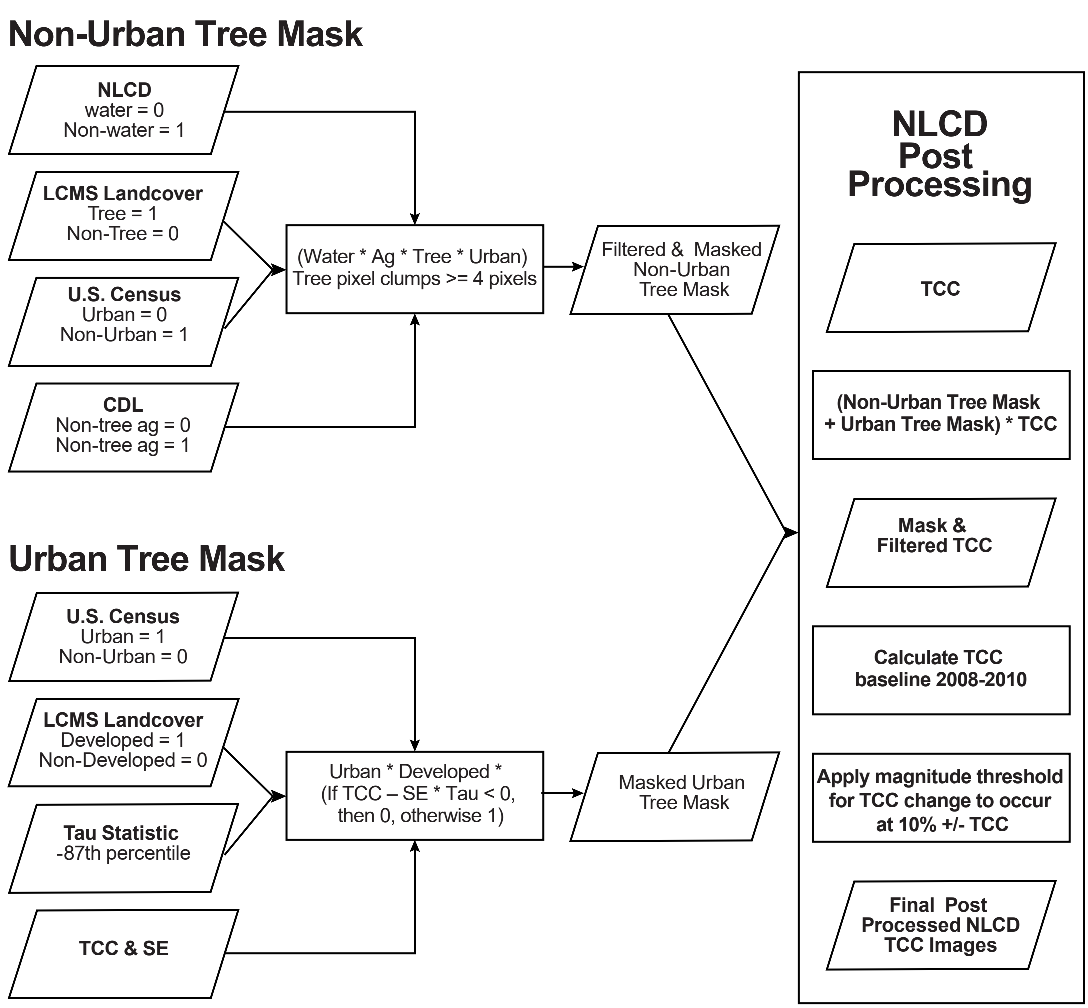

Fig. 4. The NLCD v2021.4 post-regression workflow.

applied a minimum change threshold of ±10 percent to each TCC observation sequentially in the time series. At observations where the minimum change threshold is met or exceeded ($TCC_{changeyr}$), the TCC_{baseyr} value is updated to reflect the most recent $TCC_{changeyr}$ value. Fig. 5 shows an example of a treed pixel's values through time before and after the change magnitude routine is applied.

2.5. Quality management

We did QAQC throughout the TCC workflow to identify localized artifacts that statistical tests alone could not. For production, the purpose of QAQC was to ensure quality of training, predictor and TCC model outputs throughout the processing chain, and to make improvements to the post-regression routine. For example, we reduced seam lines and spectral anomalies in final outputs by identifying set 1 and set 2 predictors during QAQC of medoid composites in pilot tests. We used a visualization toolkit (geeViz) to efficiently assess the quality of the TCC model outputs and ensure the data met national level quality standards (Housman). Many improvements were made to the post-regression routine because of QAQC. With QAQC we were able to ensure the masking and change threshold routines were implemented correctly. Without QAQC there would have been more artifacts in the TCC model output and the NLCD TCC product because of unresolved issues in the processing chain.

2.6. Model performance and map accuracy assessment

We assessed the TCC RF model performance with OOB metrics and conducted an independent accuracy assessment for the 2011 TCC map product. Ideally, the randomness of the RF algorithm results in unbiased OOB estimators of model accuracy. However, because samples are used repeatedly to create decision trees and derive OOB metrics, OOB results can be biased and should not be used for map accuracy assessment purposes (Bylander, 2002; Mitchell, 2011; Cánovas-García et al., 2017).

2.6.1. Model performance metrics

The RF algorithm withholds approximately 37 percent of the training data to use for OOB model performance metrics (R Core Team, 2020). We extracted the OOB Root Mean Square Deviation (RMSD) (Equation (2)) and Percent Variance Explained (PVE) (Equation (3)) for each of the 108 RF models in R, even though they were not used to produce mapped products (see section 2.3.3).

$$RMSD = \sqrt{\frac{\sum (Observed - Predicted)^2}{Number\ of\ Samples}} * 100 \qquad \text{Equation 2}$$

$$PVE = \left(1 - \frac{\sum (Observed - Predicted)^2}{\sum (Observed - \overline{Observed})^2}\right) * 100 \qquad \text{Equation 3}$$

2.6.2. Map validation

Traditional methods for assessing map accuracy emphasizes the use of independent data for map validation purposes, these data are not used to train or calibrate the model (Congalton and Green, 2008; Foody, 2002; Stehman and Foody, 2019). Accordingly, we withheld a randomly selected 30 percent of the final CONUS reference data (16,607 plots) to

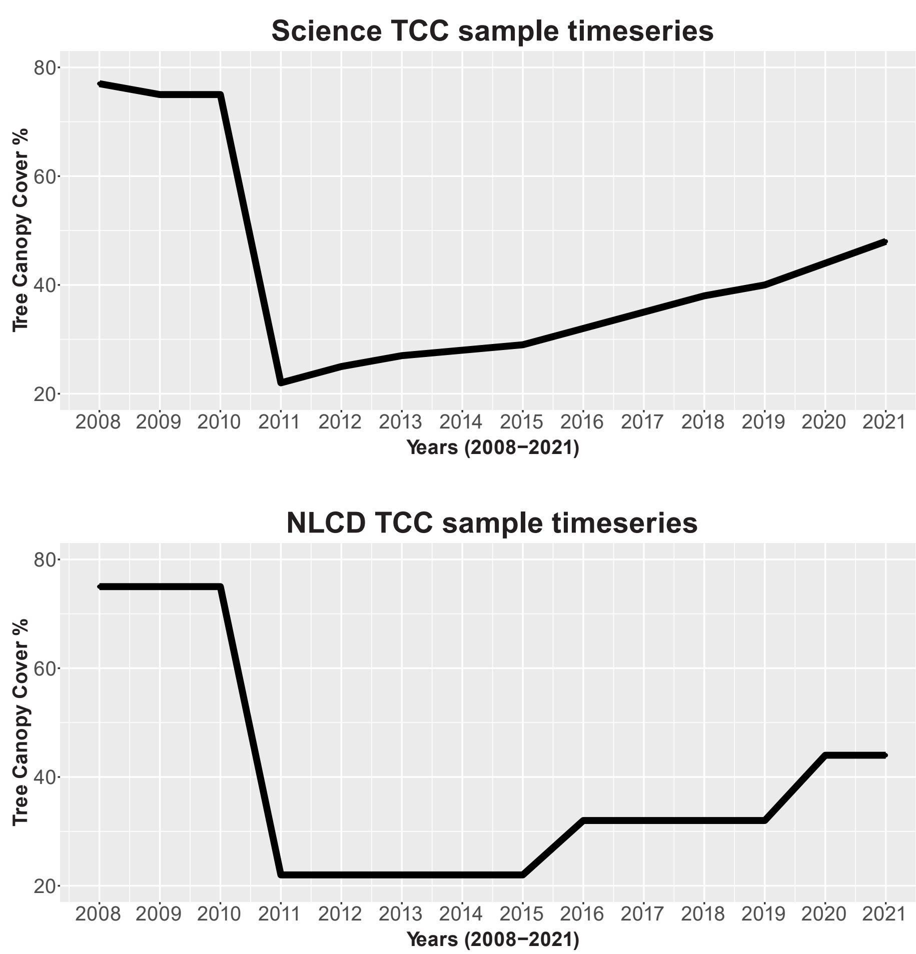

Fig. 5. For a given pixel, a sample Science (a) and NLCD (b) TCC time series from 2008 to 2021. The NLCD TCC value was updated three times when TCC change exceeded +10 percent compared to the 77 percent TCC baseline – in 2011, 2016, and 2020.

use for the map accuracy assessment.

Spatially unbalanced validation datasets can lead to biased accuracy assessment if they do not representatively sample the phenomenon of interest or use methods that account for representative area weights (Stehman and Foody, 2019). The FIA base grid is a spatially balanced sampling design that enables probabilistic estimates, is representative of US forests populations, is spatially balanced within FIA estimation units, and robustly allows the collection of different intensities in different geographies per partner needs (Reams et al., 2005). While the FIA photointerpretation collect for the TCC project is spatially balanced across FIA estimation units, for this accuracy analysis the data are used at a national scale which exhibits varying spatial densities across states; therefore, estimators need to account for the varying spatial weights (density) of the data. To create a nationally coherent set of area weights per plot that accounts for locations dropped during reference data refinement, we developed a GIS routine to assign area weights to each validation plot to calculate a weighted-by-area root mean square deviation ($RMSD_w$). Thiessen polygons were created for each holdout validation plot location. Thiessen polygons on the borders of CONUS extended far beyond CONUS extents, so we calculated their area from the neighboring polygons mean area. We used a set of three levels of geographic neighbor sets to calculate the mean: the first set was non-border polygons immediately adjacent to the border polygons; the second set was polygons immediately adjacent to the first set; the third set was polygons adjacent to the second set. The polygon area corresponding to each validation plots was used to calculate the $RMSD_w$ as shown in Equation (4) and the weighted mean absolute error (MAE_w) using Equation (5).

$$RMSD_w = \sqrt{\frac{\sum (Predicted\ TCC - Observed\ TCC)^2 * Plot\ Area}{\sum Plot\ Area}} \quad \text{Equation 4}$$

$$MAE_w = \frac{\sum abs(Predicted\ TCC - Observed\ TCC) * Plot\ Area}{\sum Plot\ Area} \quad \text{Equation 5}$$

3. Results

The NLCD TCC v2021.4 product suite includes wall-to-wall maps of spatially and temporarily consistent TCC data ready to use in a variety of applications (Fig. 6). These data and Tau confidence percentiles are available for download from the Multi-Resolution Land Characteristics consortium website (Multi-Resolution Land Characteristics Consortium) and archived with full documentation in the Forest Service geodata clearinghouse (USDA Forest Service). Tau, which was first delivered in the v2021.4 data release, can be used to meet a variety of users' needs, such as constructing confidence intervals around TCC predictions or in custom tree masking routines. Data viewing and clipping are enabled in the Multi-Resolution Land Characteristics consortium online viewer (Multi-Resolution Land Characteristics Consortium) and big data applications can take advantage of TCC data in the cloud through the GEE data catalog (USDA Forest Service Geospatial Technology and Applications Center (GTAC)). Details on technical product changes between minor version releases are reported at the time of product release to update users.

3.1. Model performance metrics

The TCC set1 and set2 RF models were compared for each of the 54 equal-area tiles, both OOB RMSD and PVE model performance metrics (equations (2) and (3)) (Table 1 and Fig. 7) (see section 2.3 for TCC model details). The largest difference between model performance within a single tile was 0.2 for RMSD and 0.4 for PVE; average difference between set1 and set2 model performance metrics within tiles was 0.08 for RMSD and 0.20 for PVE. Across the CONUS RF TCC models, mean RMSD is 12.2 for both model sets, with an overall range of 14.4–9.6. Across the CONUS RF TCC models, mean PVE is 83, with a high of 90 and a low of 60. Western and Eastern model results are differentiated to allow general regional comparisons, where Western tiles include all tiles south and west of North Dakota (tile 46 in Fig. 2).

Fig. 6. The wall-to-wall CONUS NLCD TCC map in year 2021. Science TCC v2021.4 data are available annually for years 2008–2021. The CONUS NLCD TCC v2021.4 data are available annually for years 2011–2021.

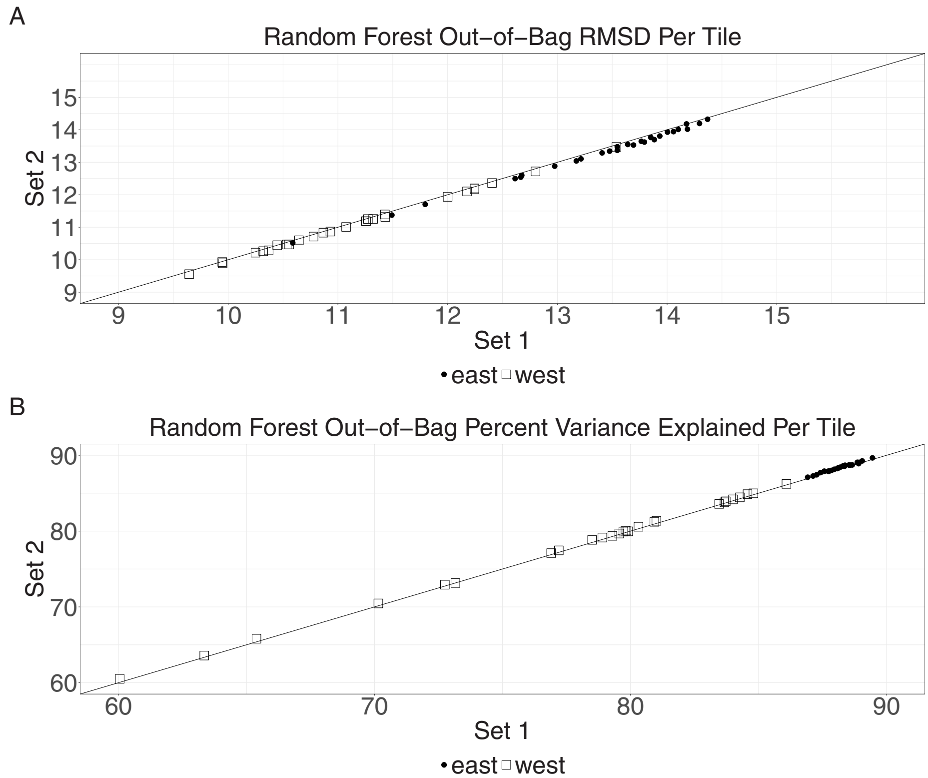

Fig. 7. Comparison of the RF model performance metrics for two sets of 2011 TCC models used to map TCC in 54 equal-area tiles across CONUS. Values for the Western tiles are squares and values for the Eastern tiles are black dots, where Western tiles include all equal-area tile units south and west of North Dakota or tile 46 in Fig. 2. The 1-to-1 line is shown in light gray.

3.2. Model standard error

We sampled a random one percent of pixels from the 2011 Science TCC CONUS map to determine if model predictions varied between the Eastern and Western CONUS. The random sample suggests model predictions in the East had larger SE ranges than in the West (Fig. 8). SE for Eastern and Western model results were lowest where the models predicted no-tree cover (zero percent).

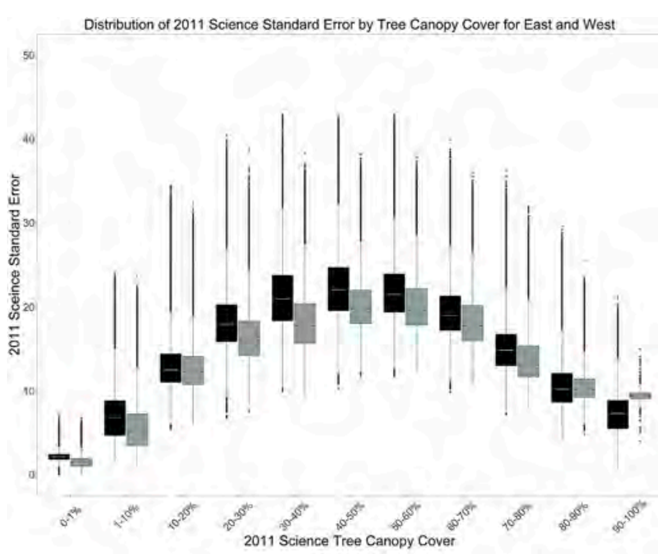

Fig. 8. Display of per-pixel TCC and SE from Western and Eastern CONUS mapping tiles where Western tiles include all tiles south and west of North Dakota (tile 46 in Fig. 2). The x-axis are bins of TCC at ten percent intervals and the y-axis are SE. The lines within the boxes represent the median SE. The data (100,744,490 values) are approximately one percent random sample of the CONUS pixels.

Fig. 9 is a comparison of TCC and SE data from this current release (v2021.4) to the TCC and SE data of the previous TCC release (v2019) of Science (A, C) and post-regression (NLCD) (B, D) for map year 2011 (A, B) and 2016 (C, D).

3.3. Map accuracy

We conducted an independent map accuracy assessment for the 2011 NLCD TCC v2021.4 map using the 16,607 plots excluded from the model training datasets (see section 2.1). Using a Thiessen polygon weighting routine per plot, we calculated $RMSD_w$ and MAE_w using equations (2) and (3) as described in section 2.6.2. The CONUS TCC map at the level of a national summary had a $RMSD_w$ of 12.8 and MAE_w of 8.0.

3.4. Example applications

The TCC workflow was redesigned to improve the temporal and spatial coherency of the TCC products to improve their ability to support inventory and monitoring applications. Here we provide several selected examples of how TCC data can be used to address landscape wide analysis for both exploration and decision support.

TCC loss and gain through time are evidence of spatiotemporal patterns caused by various natural disturbance and human activity events. In three localized case areas, the new TCC time-series data depict changing status of TCC before and after wildfire events (USDA Forest Service and US Geological Survey) and change events that appear to be timber harvests (Fig. 10). A key feature of continuous TCC data is that they offer more information than a simple binary or thematic “change” or “no change” class, while also providing spatiotemporal patterns. The percent TCC visibly drops following each event, sometimes a fraction of

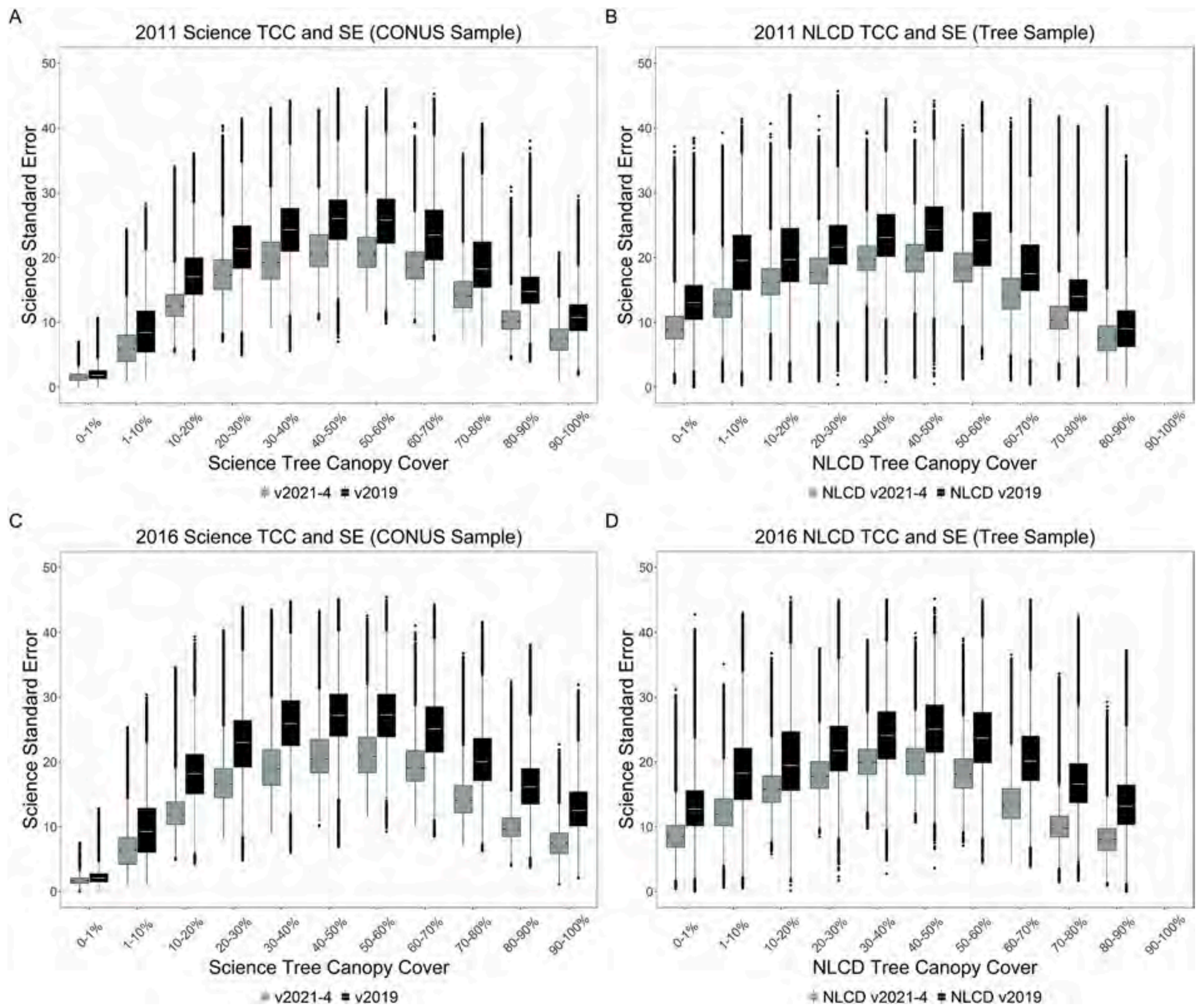

Fig. 9. A random sample of 100,744,490 (approximately one percent of the CONUS) pixels were used to compare the current (2021-4) and previous release (v2019) of Science (A, C) and NLCD or post-regression (B, D) TCC and SE data and data for map year 2011 (A, B) and 2016 (C, D).

the original percent TCC and sometimes a stand clearing event. The data yield information on the amount of relative change in percent canopy cover through time along with spatiotemporal patterns.

A second key feature of these new TCC data is their temporal and spatial coherence which supports broad-scale status and trends in treed landscapes. We show how these TCC time-series data can provide nuanced information for monitoring TCC before and after individual disturbance events, natural disasters, and targeted management activities. The impacts of the catastrophic 2016 wildfire in Gatlinburg, Tennessee can be seen through the changes in both amount and arrangement of TCC (Fig. 11). The fire's impact is seen in the Monitoring Trends in Burn Severity burn perimeter and TCC time series. Prior to the fire, tree canopy covered approximately 80 percent of the area within the fire perimeter. After the 2016 wildfire event, TCC decreased 60 percent in absolute terms (75 percent in relative terms) and tree canopy covered only 20 percent of the total area. Post-fire, TCC gradually recovers within the burned area. Characterizing the degree of change, both loss and gain, in the percent tree cover at annual time-steps has real and practical implications for forest conditions, fire prevention, restoration planning, erosion control, water quality, and the potential for salvage logging.

Finally, in this example, we explore temporal and change magnitude trends in TCC at broader ecoregion due to wildfires (Fig. 12). We used all wildfire burn boundaries across the CONUS between 2010 and 2017 from the Monitoring Trends in Burn Severity data set (USDA Forest Service and US Geological Survey). We normalized TCC time series to the Monitoring Trends in Burn Severity wildfire year, graphing TCC annual values so that x-axis values less than zero include TCC plots from years before the wildfire, and x-axis values greater than zero depict TCC plots in the years after the wildfire. In this analysis, in all regions at least one fire event had a TCC record of event +8 years. We grouped the fire event year normalized TCC trends by Environmental Protection Agency (EPA) level 1 ecoregions to explore the impacts of wildfire events across ecosystem scales (Omernik and Griffith, 2014). The highest mean ecoregion TCC occurs in the Marine West Coast Forests ecoregion, which also showed the largest absolute decrease in magnitude of TCC during the post-fire period. This analysis demonstrates how the time-series of TCC data can capture broad-scale tree vegetation responses to wildfire. These data can support additional broad-scale analyses to explore the impacts of different fire disturbance regimes on TCC, the average severity (measured by decreases in TCC) by fire year in each ecoregion and whether it has changed through time, and temporal data about the growth rates of TCC after fire relative to fire size and severity.

4. Discussion

This manuscript presents the methods investigations, processing workflow, QAQC practices, and results from a new generation of annual NLCD TCC maps (v2021.4). The techniques to map spatially continuous national TCC with satellite data have been improving for decades

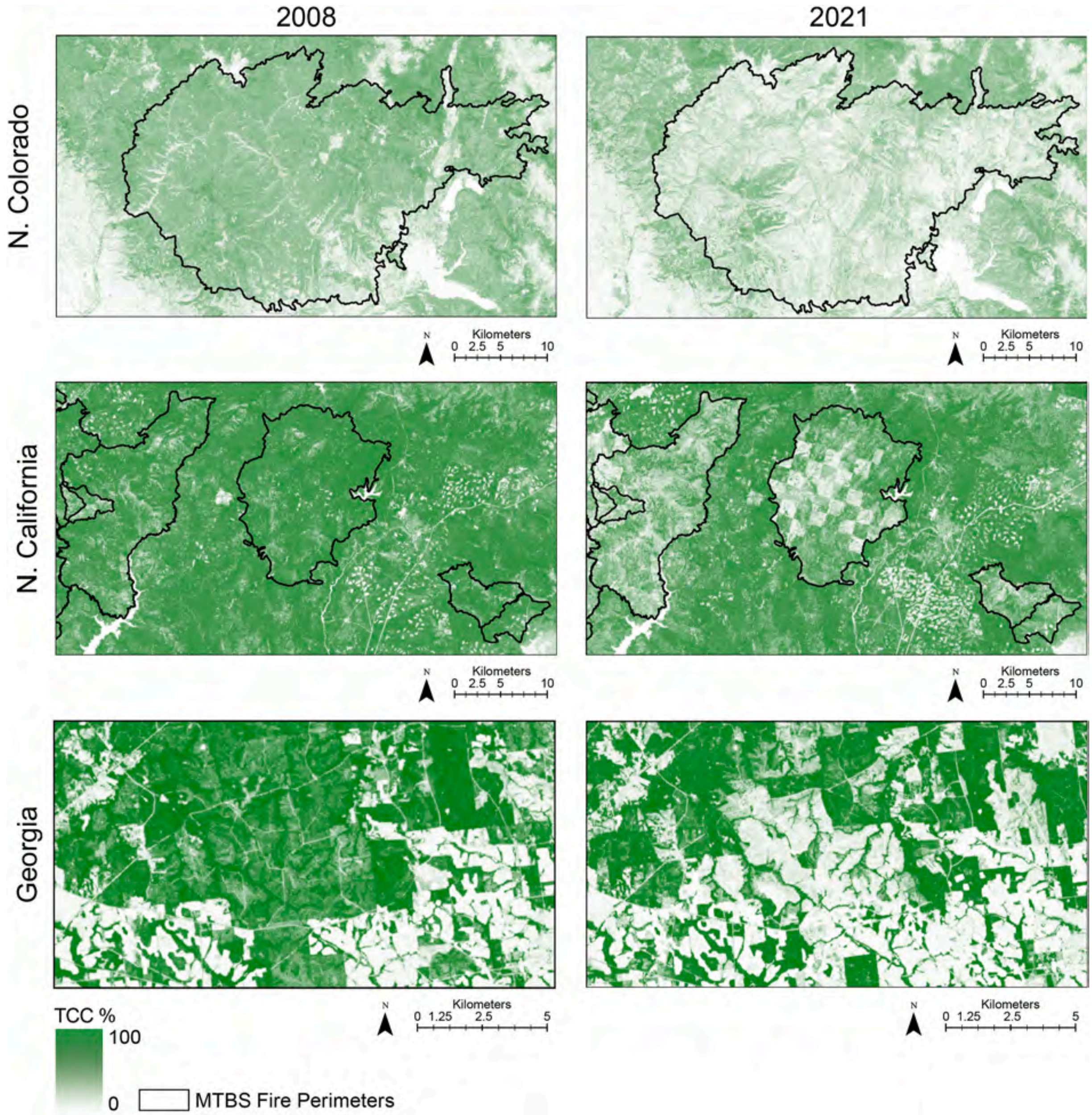

Fig. 10. Left images are TCC in 2008 and the right images are TCC in 2021. The top row shows TCC before and after the East Troublesome fire in northern Colorado. The middle row shows TCC before and after wildfire and mechanical/timber harvest of TCC in northern California. The bottom row shows TCC before and after mechanical/timber harvest in Georgia.

(DeFries et al., 1999; Huang et al., 2001; Hansen et al., 2002; Sannier et al., 2023; Egorov et al., 2023; Harrison et al., 2025; Sexton et al., 2013). Still, the annual NLCD TCC data are unique in their combination of strengths. First, the new workflows support a "collections" approach, where the entire record is updated after changes to the established processing workflow. This approach prioritizes the length and coherency of the annual TCC records. Products that do not take this or a similar approach to temporal coherency may confound methodological change with true change, making data comparisons through time challenging. Second, the continuous annual TCC products meet the need for national and international forest reporting and monitoring because the reference data (and or definitions for classification) used to calibrate and assess models and final map products, are harmonized with the definitions of the USDA Forest Service and represent the full range of TCC (0–100 percent) (Zalles et al., 2024). Coherent uninterrupted time-series of continuous (0–100 percent) TCC data offer additional information over annual, categorical maps of forest cover for management and policy (Vogt et al., 2024; Betts et al., 2024). Yet, most time-series mapping continues to focus on coarse classes of categorical forest cover through time (Sohl et al., 2025). Third, the reference data used to assess final maps, uses a statistical national all-ownership and all-lands sample design – the FIA annual inventory (Ruefenacht et al., 2022; Bechtold and Patterson, 2005). Tree cover or forest map assessments not based on such a probabilistic design may introduce bias into accuracy assessments. Fourth, including timely map accuracy and true model uncertainty metrics, such as Tau (τ), is critical for data-driven natural resource management decisions. Finally, the application of robust accuracy and uncertainty techniques to these data and reported (in metadata and technical docs) at time of release are an important step forward in total project QAQC.

We met project goals to produce spatially and temporally continuous data (annual time-steps), improve product reproducibility and quality,

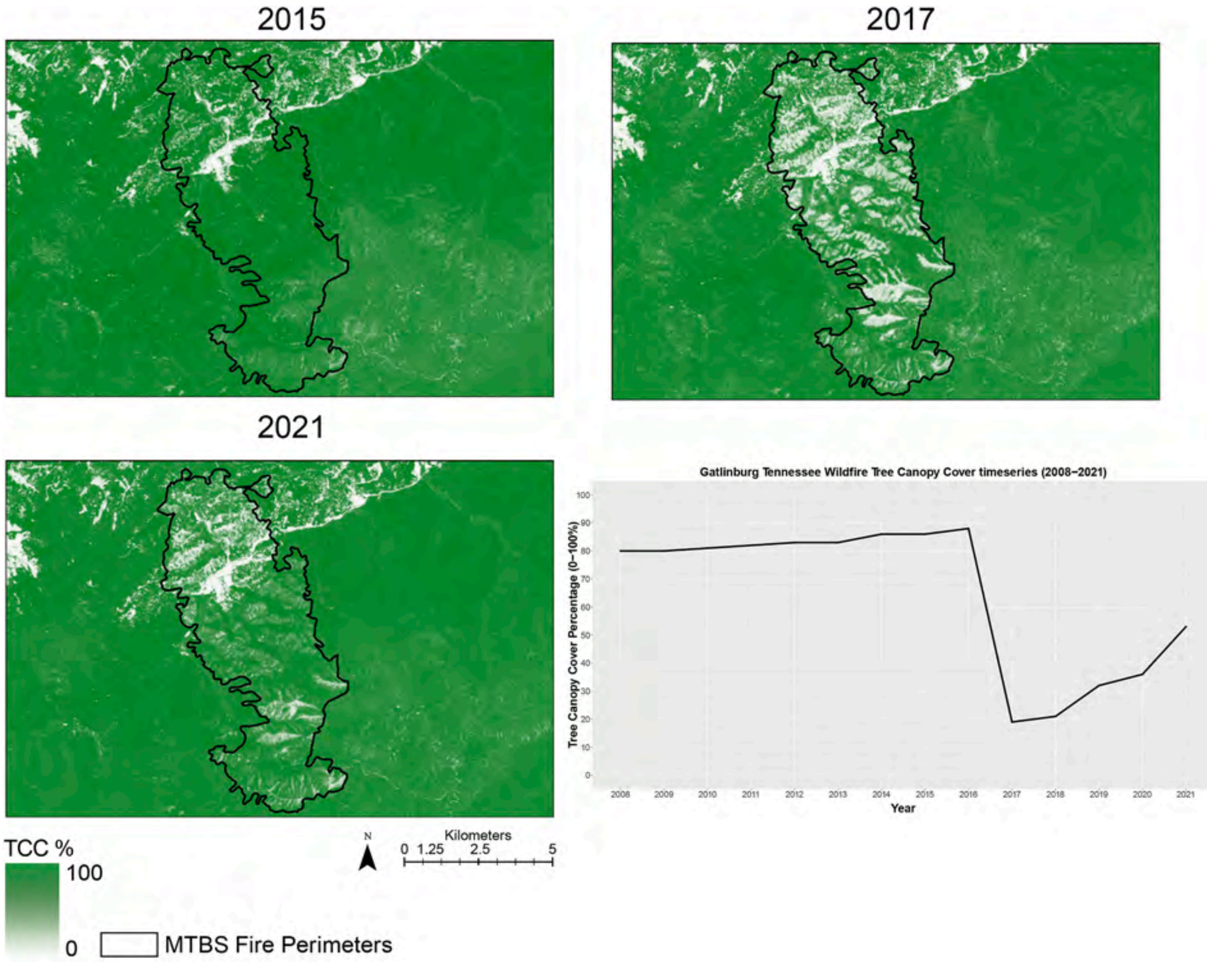

Fig. 11. Maps of a 2016 wildfire event in Gatlinburg Tennessee. The upper left map is TCC in 2015, before the wildfire. The upper right map is TCC in 2017, the year after the fire. The lower left map is TCC in 2021, showing TCC gain l the years following the fire.

decrease product release latency, and reduce costs through a combination of new approaches. This workflow allows for the release of new CONUS annual TCC time-series data within 6 months of the last satellite image capture (end of growing season of previous year). We used the GEE cloud computing environment for image processing, model predictions, and post-regression routines, overcoming computation and storage challenges in previous TCC workflows. Availability of USGS Collection 2 Landsat Tier 1 and Sentinel-2 (A/B) Level-1C top-of-atmosphere reflectance imagery in the GEE data catalog and the geeViz Python library allowed us to effectively process thousands of Landsat and Sentinel scenes and generate annual composites (1984–2022) (Housman). National composites smoothed with the LandTrendr algorithm, reduced seam lines and spectral anomalies in final products. The moving window approach, where for each center tile a RF model was trained on reference data and predictors within a 5x5 window of equal-area tiles (480 × 480 km) then applied to the center tile, allowed for 30 percent holdout of reference data (16,607 plots) without compromising model performance. An independent statistical assessment of the CONUS 2011 TCC map yielded an $RMSD_w$ of 12.8 and MAE_w of 8.0. Incorporating a time-invariant modeling approach enabled production of annual TCC time-series without new reference data collection. In this framework, we trained models on the relationships between 2011 FIA photo-interpreted reference data and 2011 predictor data, then applied the 2011 models to other years in the predictor time-series. It is critical with model temporal transfer that the assumption of temporal consistency in model inputs remain intact throughout the time series. Vogeler et al. (2020) proved this assumption could be met even as Landsat sensor characteristics change from Multispectral Scanner to Landsat 8. A recent study demonstrated that under temporal transfer LandTrendr smoothed Landsat time-series predictors produced more accurate model predictions than using non-smoothed composites (Filippelli et al., 2024).

Results demonstrate the ability of time-invariant model approach to produce stable TCC predictions for other years in the time series even with two predictor sets. Image quality and availability through time forced the use of two sets of predictors and two sets of models (to accommodate Landsat 7 scan-line related issues between 2003 and 2015) and a narrowing of the growing season window filter (starting in 2016). Pilot testing over four pilot areas from diverse ecosystems showed no major shifts in model TCC residual values through time (Fig. 3). CONUS-wide results show the consistency in the pattern and magnitudes of model SE over ranges of TCC, in years 2011 and 2016, for all sampled pixels (Fig. 9A and C) and for all sampled pixels in treed areas (NLCD TCC) (Fig. 9B and D).

Model performance metrics also indicate that the time-invariant modeling approach was not compromised by the inclusion of two sets of models. Specifically, OOB model performance results comparing the two sets of 2011 models within each tile show a near 1:1 relationship (Fig. 7). Comparisons between the 54 equal-area tiles, find trends for RMSD and PVE OOB for both model sets almost identical: RMSD ranges from 14.4 to 9.6 (set1) and 14.3–9.6 (set 2) with a median of 12.3, and PVE ranges from 60.1 to 89.5 (set1) and 60.5 to 89.7 (set2) with a median of 86.7. Finally, visual quality assessments of mapped TCC and SE annual results also found limited anomalies through the time series.

Fig. 12. TCC temporal records averaged over MTBS burn boundaries show TCC values drop post-fire events in both forest and non-forest dominated Environmental Protection Agency (EPA) level 1 ecoregions (USDA Forest Service and US Geological Survey). MTBS burn boundaries from 2010 to 2017, were used to ensure two years of TCC Science product data were included before a potential burn in 2010, and five years of data were included following a burn. For example, if a burn occurred in 2017, there would be five years of data from 2017 to 2021. Value 0 on the x-axis is the TCC mean at the burn event year. Negative x-axis values are the TCC mean in N years before the burn. For example, x-axis value −2 is the TCC mean two years before the burn (x-axis 0). Positive x-axis values are the TCC mean in N of years after the burn. For example, x-axis value 2 is the TCC mean two years after the burn (x-axis 0).

Model performance improved from previous TCC releases. Model outputs had lower SE median, quartile, min and max values across TCC ranges (Fig. 9 black and gray bars). Median RMSD (12.3) and PVE (86.7) for the 2011 v2021.4 model sets are an improvement compared to the NLCD TCC v2019 release (Ruefenacht et al., 2022). Distinguishing between Western and Eastern CONUS TCC model performance per tile allows general regional comparisons. Western regions have lower model SE in all but the 80–90 percent and 90–100 percent canopy cover bins, which occur less frequently in the predominantly dry Western landscapes (Fig. 8). In general, Western model performance has lower median RMSD and PVE than those of Eastern tiles (Fig. 7). The PVE model min and max are lower in the Western regions (from 60 to 86) than the Eastern regions (87.1–89.7). These PVE values indicate there is potentially more variability in the target variable (observed TCC) and the models' ability to account for that variability in the Western regions compared to the Eastern regions.

To improve quality management we invested in robust quality assurance, assessment, and control approaches that are challenging to quantify as a traditional result. A systematic approach to quality assurance and use of best practices are key for every step of the project chain to ensure these Federal Geographic Data Asset datasets maintain and improve efficiency and quality of data for users. These approaches included: clear input from management partners, detailed planning in product design and process development, rigorous data quality checks throughout the processing chain, planning and implementing rigorous pilot testing of all new workflow components individually from start to end (e.g., medoid composite testing to mitigate quantity and impact of image gaps in the time series), using visualization toolkits (e.g., geeViz) for rapid exploration and analysis of TCC outputs, and planning and implementing quantitative routines to ensure model outputs meet quality standards at the national level (including releasing map accuracy assessments, multiple model uncertainty metrics, and rigorous process documentation and control). These approaches were designed to create a quality system to support subsequent product runs, ensure future TCC products and processes can proactively address issues, drive continuous improvements, and advance customer satisfaction. Additional project benefit in switching to open-source cloud-based production are the contributions made to open-source code libraries, training, and modern computation techniques improving the available scientific knowledge base. While it is common to make statements of the incredible number of pixels processed per second to produce a map product of this breadth, our experience indicates more attention should be given to investing in systems that leverage strengths of humans-in-the-loop to produce quality vegetation maps at large extents that serve management and policy needs (Wu et al., 2022). Repeatedly, we find that analysts identify localized artifacts in outputs that statistical tests do not.

Examples of applications with these TCC data illustrate how the nationwide annual TCC v2021.4 data can meet a variety of users' needs and enable new practical applications of inventory and monitoring data. These temporally and spatially coherent continuous TCC data depict changes in the forest condition (direction and magnitude) of TCC, characterizing non-stand replacing events. This information can complement emerging national change attribution data sets to meet needs for an ecological perspective on disturbance regimes (Betts et al., 2024; Kennedy et al., 2014; Stahl et al., 2023).

There are limitations on the appropriate use of these annual NLCD TCC data. For example, when using these maps to report areal extents, statistical estimators should be used rather than pixel summing (zonal) techniques in most cases (Waldner and Defourny, 2017; Francini et al., 2022; Greenfield and Schleeweis, 2023). Also, challenges with relying only on moderate resolution TCC maps in regions with highly heterogenous land-cover are known and assessments of prior NLCD TCC products were shown to exhibit increasing underestimation of TCC and increased spatial error increased with increasing urban density (Heris et al., 2022).

We identified improvements to make to subsequent NLCD TCC data releases. First, using the methods presented with only slight modifications, we improved the interannual coherency of the TCC time-series by extending annual TCC data back to 1985 in the Science and NLCD TCC v2023.5 (1985–2023) products (Housman et al., 2025). The v2023.5 data can be downloaded from the US Forest Service geodata clearinghouse or GEE (USDA Forest Service). Next, we noticed seam lines between Great Plains and Midwest tiles where there are Science TCC differences over highly productive crops such as corn. For the Science TCC v2023.5 product, TCC differences were lessened over crops between problematic tiles by modifying our moving window modeling approach for the problem tiles. Finally, in certain areas our quality assessments revealed notable differences in SE and TCC between 2015 and 2016, when our image acquisition date range narrowed, and Sentinel-2 imagery became available. For the NCLD TCC v2023.5 product, we modified the urban tree mask by adjusting the Tau (τ) value confidence percentile between 2015 and 2016, resulting in less SE and TCC differences between those years.

There were issues identified in the v2021.4 data that persisted in the v2023.5 data. The v2021.4 data $RMSD_w$ of 12.8 and MAE_w of 8.0, suggest there are localized areas with larger map errors. The $RMSD_w$ metric gives more weight to outliers and is a useful descriptor when large errors are especially undesirable. The MAE_w is a simpler description of the average errors without consideration of whether the errors are large or small. When errors are uniformly distributed MAE_w and $RMSD_w$ are similar. Future improvements could expand the map accuracy assessment to include temporal cross-validation, multiscale spatial assessment across ranges of TCC, and provide explicit metrics on change in both magnitude and direction of TCC through time (Stehman and Foody, 2019; Riemann et al., 2010; Pontius et al., 2025). Doing so would better inform users' on when and where TCC products meet the suitability requirements for their applications. Furthermore, time-invariant temporal transfer can result in increased model bias through time (Filippelli et al., 2024). Research investigations are underway to test the efficacy of expanding reference data years using more FIA reference data used, and/or augmenting the FIA sample with nation-wide airborne LiDAR data or crowd-sourced photointerpretation for time-agnostic modeling. Recent work by Corro et al. (2025) with the NLCD TCC v2021.4 products demonstrate methods to enhance the NLCD TCC thus improving the accuracy of TCC within urban areas. Finally, production efforts are underway to increase user access to Science and NCLD TCC data for exploration and geospatial analysis in a cloud-based platform. The goal of this effort is to empower TCC data users that include policy and land managers, with an easy-to-use online environment where they can leverage the TCC data to make informed land management decisions.

5. Conclusions

This generation of the nationwide annual NLCD TCC v2021.4 (2011–2021), produced by the USDA Forest Service and attributed to the USGS NLCD product suite, meets user community and stakeholder defined needs. The workflow presented reduced development costs, increased production speed, minimized subjective analyst interaction, improved data and process quality through quality management measures, and improved product release latency rate. Recently, this robust workflow was used to expand annual NLCD TCC products back to 1985, in the most recent NLCD TCC data release v2023.5, to further support information needs on the status (inventory) and trends (monitoring) of TCC. This Federal Geographic Data Asset dataset in the Land Cover and Land Use Change theme is delivered through a unique inter-agency collaboration between USDA Forest Service and the Department of Interior USGS as members of the Multi-Resolution Land Characteristics consortium. The authoritative data provides a unique and complimentary information source for the many public and private customers of the annual NLCD product suite.

CRediT authorship contribution statement

Joshua Heyer: Writing – review & editing, Writing – original draft, Visualization, Validation, Software, Methodology, Investigation, Formal analysis, Data curation, Conceptualization. **Karen Schleeweis:** Writing – review & editing, Writing – original draft, Validation, Supervision, Project administration, Methodology, Investigation, Funding acquisition, Conceptualization. **Bonnie Ruefenacht:** Writing – review & editing, Writing – original draft, Visualization, Validation, Software, Methodology, Investigation, Data curation. **Ian Housman:** Writing –

review & editing, Writing – original draft, Visualization, Software, Methodology, Investigation, Formal analysis, Data curation, Conceptualization. **Yang Zhiqiang:** Writing – review & editing, Software. **Daniel Ryerson:** Writing – review & editing, Supervision, Resources, Project administration, Methodology, Investigation, Data curation, Conceptualization. **Jaclyn Reischmann:** Writing – review & editing, Supervision, Project administration, Methodology. **Kevin Megown:** Writing – review & editing, Supervision, Resources, Investigation, Funding acquisition, Conceptualization. **M. Seth Bogle:** Writing – review & editing, Validation, Supervision, Resources, Project administration.

Ethical responsibilities of authors

All authors have read, understood, and complied as applicable.

Funding

This work was supported by the U.S. Department of Agriculture Forest Service National Forest System and Research and Development.

Declaration of competing interest

The authors declare the following financial interests/personal relationships which may be considered as potential competing interests: Joshua Heyer reports financial support and article publishing charges were provided by U.S. Department of Agriculture Forest Service National Forest System and Research and Development. If there are other authors, they declare that they have no known competing financial interests or personal relationships that could have appeared to influence the work reported in this paper.

Acknowledgements

The Forest Inventory and Analysis Program data used in or as part of this project were made possible, in part, through an Agreement within the United States Department of Agriculture's Forest Service. We would like to thank the reviewers from Science of Remote Sensing whose contributions enhanced the quality of the paper. The TCC 2021.4 product would not be possible without the work done by the Google Earth Engine team at Google, and Mark Finco, Wendy Goetz, and Vicky Johnson for their contributions to the methodological development of the TCC product.

Appendix A. Supplementary data

Supplementary data to this article can be found online at https://doi.org/10.1016/j.srs.2025.100301.

Data availability

TCC data are available on the USFS Raster Gateway and in Google Earth Engine. FIA reference data are confidential and not publicly available. Non-proprietary USFS code and predictor data are available upon request.

References

Bechtold, W.A., Patterson, P.L. (Eds.), 2005. The Enhanced Forest Inventory and Analysis Program - National Sampling Design and Estimation Procedures. U.S. Department of Agriculture, Forest Service, Southern Research Station, Asheville, NC. https://doi.org/10.2737/SRS-GTR-80. Gen. Tech. Rep. SRS-80. (Accessed 30 April 2025).

Berryman, E., McMahan, A., 2019. Chapter 7 - using tree canopy cover data to help estimate acres of damage. In: Potter, K.M., Conkling, B.L. (Eds.), Forest Health Monitoring: National Status, Trends, and Analysis 2018. Gen. Tech. Rep. SRS-239. U. S. Department of Agriculture, Forest Service, Southern Research Station, Asheville, NC, pp. 125–141. https://research.fs.usda.gov/treesearch/58747. (Accessed 29 April 2025).

Betts, M.G., Yang, Z., Hadley, A.S., Hightower, J., Hua, F., Lindenmayer, D., Seo, E., Healey, S.P., 2024. Quantifying forest degradation requires a long-term, landscape-scale approach. Nat. Ecol. Evol. 8, 1054–1057. https://doi.org/10.1038/s41559-024-02409-5.

Boryan, C., Yang, Z., Mueller, R., Craig, M., 2011. Monitoring US agriculture: the US department of agriculture, National Agricultural Statistics Service, Cropland Data Layer Program. Geocarto Int. 26, 341–358. https://doi.org/10.1080/10106049.2011.562309.

Breiman, L., 2001. Random forests. Mach. Learn. 45, 5–32. https://doi.org/10.1023/A:1010933404324.

Brown, J.F., Tollerud, H.J., Barber, C.P., Zhou, Q., Dwyer, J.L., Vogelmann, J.E., Loveland, T.R., Woodcock, C.E., Stehman, S.V., Zhu, Z., Pengra, B.W., Smith, K., Horton, J.A., Xian, G., Auch, R.F., Sohl, T.L., Sayler, K.L., Gallant, A.L., Zelenak, D., Reker, R.R., Rover, J., 2020. Lessons learned implementing an operational continuous United States national land change monitoring capability: The Land Change Monitoring, Assessment, and Projection (LCMAP) approach. Remote Sens. Environ. 238, 111356. https://doi.org/10.1016/j.rse.2019.111356.

Buchhorn, M., Lesiv, M., Tsendbazar, N.-E., Herold, M., Bertels, L., Smets, B., 2020. Copernicus global land cover layers—collection 2. Remote Sens. 12, 1044. https://doi.org/10.3390/rs12061044.

Bylander, T., 2002. Estimating generalization error on two-class datasets using out-of-bag estimates. Mach. Learn. 48, 287–297. https://doi.org/10.1023/A:1013964023376.

Cánovas-García, F., Alonso-Sarría, F., Gomariz-Castillo, F., Oñate-Valdivieso, F., 2017. Modification of the random forest algorithm to avoid statistical dependence problems when classifying remote sensing imagery. Comput. Geosci. 103, 1–11. https://doi.org/10.1016/j.cageo.2017.02.012.

Chastain, R., Housman, I., Goldstein, J., Finco, M., Tenneson, K., 2019. Empirical cross sensor comparison of Sentinel-2A and 2B MSI, Landsat-8 OLI, and Landsat-7 ETM+ top of atmosphere spectral characteristics over the conterminous United States. Remote Sens. Environ. 221, 274–285. https://doi.org/10.1016/j.rse.2018.11.012.

Congalton, R.G., Green, K., 2008. Assessing the Accuracy of Remotely Sensed Data: Principles and Practices, second ed. CRC Press.

Corro, L.M., Bagstad, K.J., Heris, M.P., Ibsen, P.C., Schleeweis, K.G., Diffendorfer, J.E., Troy, A., Megown, K., O'Neil-Dunne, J.P.M., 2025. An enhanced national-scale urban tree canopy cover dataset for the United States. Sci. Data 12, 490. https://doi.org/10.1038/s41597-025-04816-0.

Coulston, J.W., Moisen, G.G., Wilson, B.T., Finco, M.V., Cohen, W.B., Brewer, C.K., 2012. Modeling percent tree canopy cover: a pilot study. Photogramm. Eng. Rem. Sens. 78, 715–727. https://www.srs.fs.usda.gov/pubs/ja/2012/ja_2012_coulston_001.pdf. (Accessed 30 April 2025).

Coulston, J.W., Blinn, C.E., Thomas, V.A., Wynne, R.H., 2016. Approximating prediction uncertainty for random forest regression models. Photogramm. Eng. Rem. Sens. 82, 189–197. https://doi.org/10.14358/PERS.82.3.189.

DeFries, R.S., Townshend, J.R.G., Hansen, M.C., 1999. Continuous fields of vegetation characteristics at the global scale at 1-km resolution. J. Geophys. Res. Atmos. 104, 16911–16923. https://doi.org/10.1029/1999JD900057.

Dewitz, J., Geological Survey, U.S., 2021. National Land Cover Database (NLCD) 2019 Products (ver. 3.0, February 2024). U.S. Geological Survey Data release. https://doi.org/10.5066/P9KZCM54.

Díaz, S., Demissew, S., Carabias, J., Joly, C., Lonsdale, M., Ash, N., Larigauderie, A., Adhikari, J.R., Arico, S., Báldi, A., Bartuska, A., Baste, I.A., Bilgin, A., Brondizio, E., Chan, K.M., Figueroa, V.E., Duraiappah, A., Fischer, M., Hill, R., Koetz, T., Leadley, P., Lyver, P., Mace, G.M., Martin-Lopez, B., Okumura, M., Pacheco, D., Pascual, U., Pérez, E.S., Reyers, B., Roth, E., Saito, O., Scholes, R.J., Sharma, N., Tallis, H., Thaman, R., Watson, R., Yahara, T., Hamid, Z.A., Akosim, C., Al-Hafedh, Y., Allahverdiyev, R., Amankwah, E., Asah, S.T., Asfaw, Z., Bartus, G., Brooks, L.A., Caillaux, J., Dalle, G., Darnaedi, D., Driver, A., Erpul, G., Escobar-Eyzaguirre, P., Failler, P., Fouda, A.M.M., Fu, B., Gundimeda, H., Hashimoto, S., Homer, F., Lavorel, S., Lichtenstein, G., Mala, W.A., Mandivenyi, W., Matczak, P., Mbizvo, C., Mehrdadi, M., Metzger, J.P., Mikissa, J.B., Moller, H., Mooney, H.A., Mumby, P., Nagendra, H., Nesshover, C., Oteng-Yeboah, A.A., Pataki, G., Roué, M., Rubis, J., Schultz, M., Smith, P., Sumaila, R., Takeuchi, K., Thomas, S., Verma, M., Yeo-Chang, Y., Zlatanova, D., 2015. The IPBES conceptual framework — connecting nature and people. Curr. Opin. Environ. Sustain. 14, 1–16. https://doi.org/10.1016/j.cosust.2014.11.002.

Dowtin, A.L., Cregg, B.C., Nowak, D.J., Levia, D.F., 2023. Towards optimized runoff reduction by urban tree cover: a review of key physical tree traits, site conditions, and management strategies. Landsc. Urban Plann. 239, 104849. https://doi.org/10.1016/j.landurbplan.2023.104849.

Drusch, M., Del Bello, U., Carlier, S., Colin, O., Fernandez, V., Gascon, F., Hoersch, B., Isola, C., Laberinti, P., Martimort, P., Meygret, A., Spoto, F., Sy, O., Marchese, F., Bargellini, P., 2012. Sentinel-2: ESAs optical high-resolution Mission for GMES operational services. Remote Sens. Environ. 120, 25–36. https://doi.org/10.1016/j.rse.2011.11.026.

Egorov, A., Roy, D.P., Boschetti, L., 2023. Generation and comprehensive validation of 30 m conterminous United States landsat percent tree cover and forest cover loss annual products. Sci. Remote Sens. 7, 100084. https://doi.org/10.1016/j.srs.2023.100084.

Filippelli, S.K., Schleeweis, K., Nelson, M.D., Fekety, P.A., Vogeler, J.C., 2024. Testing temporal transferability of remote sensing models for large area monitoring. Sci. Remote Sens. 9, 100119. https://doi.org/10.1016/j.srs.2024.100119.

Flood, N., 2013. Seasonal composite landsat TM/ETM+ images using the medoid (a multi-dimensional median). Remote Sens. 5, 6481–6500. https://doi.org/10.3390/rs5126481.

Food and Agriculture Organization of the United Nations, 2015. FRA 2015 Terms and Definitions, Forest Resources Assessment Program. Food and Agriculture Organization of the United Nations, Rome, Italy. Working Paper 180. https://www.fao.org/4/ap862e/ap862e00.pdf. (Accessed 30 April 2025).

Foody, G.M., 2002. Status of land cover classification accuracy assessment. Remote Sens. Environ. 80, 185–201. https://doi.org/10.1016/S0034-4257(01)00295-4.

Francini, S., McRoberts, R.E., D'Amico, G., Coops, N.C., Hermosilla, T., White, J.C., Wulder, M.A., Marchetti, M., Mugnozza, G.S., Chirici, G., 2022. An open science and open data approach for the statistically robust estimation of forest disturbance areas. Int. J. Appl. Earth Obs. Geoinf. 106, 102663. https://doi.org/10.1016/j.jag.2021.102663.

Freeman, E.A., Bakken, J.L., Moisen, G.G., Toney, C., Nelson, M.D., Patterson, P.L., 2024. Poststratification for Increasing Precision in Forest Inventory and Analysis Estimates in the Rocky Mountain States. In: Res. Note RMRS-RN-102. U.S. Department of Agriculture, Forest Service, Rocky Mountain Research Station, Fort Collins,CO. https://doi.org/10.2737/RMRS-RN-102. (Accessed 30 April 2025).

Friedl, M.A., Woodcock, C.E., Olofsson, P., Zhu, Z., Loveland, T., Stanimirova, R., Arevalo, P., Bullock, E., Hu, K.-T., Zhang, Y., Turlej, K., Tarrio, K., McAvoy, K., Gorelick, N., Wang, J.A., Barber, C.P., Souza, C., 2022. Medium spatial resolution mapping of global land cover and land cover change across multiple decades from landsat, front. Remote Sens. 3. https://doi.org/10.3389/frsen.2022.894571.

Gatziolis, D., 2012. Comparison of LiDAR- and photointerpretation-based estimates of canopy cover. In: McWilliams, W., Roesch, F.A. (Eds.), Monitoring Across Borders: 2010 Joint Meeting of the Forest Inventory and Analysis (FIA) Symposium and the Southern Mensurationists. e-Gen. Tech. Rep. SRS-157. U.S. Department of Agriculture, Forest Service, Southern Research Station, Asheville, NC, pp. 231–235. https://research.fs.usda.gov/treesearch/41012. (Accessed 30 April 2025).

Geological Survey, U.S., 2019. USGS 3D elevation program digital elevation model. https://developers.google.com/earth-engine/datasets/catalog/USGS_3DEP_10m. (Accessed 30 April 2025).

Geological Survey, U.S., 2024. Annual NLCD collection 1 science products. U.S. Geological Survey Data release. https://doi.org/10.5066/P94UXNTS.

Gesch, D.B., Oimoen, M.J., Greenlee, S.K., Nelson, C.A., Steuck, M.J., Tyler, D.J., 2002. The national elevation dataset, Photogramm. Eng. Remote Sens. 68, 5–11.

Gesch, D.B., Evans, G.A., Oimoen, M.J., Arundel, S., 2018. The National Elevation Dataset, ASPRS, pp. 83–110. https://www.usgs.gov/publications/national-elevation-dataset. (Accessed 30 April 2025).

Goeking, S.A., Liknes, G.C., Lindblom, E., Chase, J., Jacobs, D.M., Benton, R., 2012. A GIS-based tool for estimating tree canopy cover on fixed-radius plots using high-resolution aerial imagery. In: Morin, R.S., Liknes, G.C. (Eds.), Moving from Status to Trends: Forest Inventory and Analysis (FIA) Symposium 2012. Gen. Tech. Rep. NRS-P-105. Department of Agriculture, Forest Service, Northern Research Station, Newtown Square, PA, pp. 237–241. https://research.fs.usda.gov/treesearch/42752. (Accessed 30 April 2025).

Gong, P., Wang, Jie, Yu, Le, Zhao, Yongchao, Zhao, Yuanyuan, Liang, Lu, Niu, Zhenguo, Huang, Xiaomeng, Fu, Haohuan, Liu, Shuang, Li, Congcong, Li, Xueyan, Fu, Wei, Liu, Caixia, Xu, Yue, Wang, Xiaoyi, Cheng, Qu, Hu, Luanyun, Yao, Wenbo, Zhang, Han, Zhu, Peng, Zhao, Ziying, Zhang, Haiying, Zheng, Yaomin, Ji, Luyan, Zhang, Yawen, Chen, Han, Yan, An, Guo, Jianhong, Yu, Liang, Wang, Lei, Liu, Xiaojun, Shi, Tingting, Zhu, Menghua, Chen, Yanlei, Yang, Guangwen, Tang, Ping, Xu, Bing, Giri, Chandra, Clinton, Nicholas, Zhu, Zhiliang, Chen, Jin, Chen, J., 2013. Finer resolution observation and monitoring of global land cover: first mapping results with landsat TM and ETM+ data. Int. J. Rem. Sens. 34, 2607–2654. https://doi.org/10.1080/01431161.2012.748992.

Gorelick, N., Hancher, M., Dixon, M., Ilyushchenko, S., Thau, D., Moore, R., 2017. Google Earth engine: planetary-scale geospatial analysis for everyone. Remote Sens. Environ. 202, 18–27. https://doi.org/10.1016/j.rse.2017.06.031.

Greenfield, E.J., Schleeweis, K., 2023. Comparing the USDA forest service tree canopy cover datasets 2011, 2016, 2019 and 2021 with photointerpretation of high-resolution google Earth imagery: guidance for use in in community scale forest management. White Paper, USDA Forest Service Forest Inventory and Analysis. https://www.itreetools.org/documents/955/USFSTCCvsPIWhitePaperNovember2023.pdf. (Accessed 1 May 2025).

Guler, D., Buttenfield, B.P., Charisoulis, G., Yomralioglu, T., 2022. Comparative analysis of bioenergy potential and suitability modeling in the USA and Turkey. Sustain. Energy Techn. 53, 102626. https://doi.org/10.1016/j.seta.2022.102626.

Hansen, M.C., Loveland, T.R., 2012. A review of large area monitoring of land cover change using landsat data. Remote Sens. Environ. 122, 66–74. https://doi.org/10.1016/j.rse.2011.08.024.

Hansen, M.C., DeFries, R.S., Townshend, J.R.G., Sohlberg, R., Dimiceli, C., Carroll, M., 2002. Towards an operational MODIS continuous field of percent tree cover algorithm: examples using AVHRR and MODIS data. Remote Sens. Environ. 83, 303–319. https://doi.org/10.1016/S0034-4257(02)00079-2.

Hansen, M.C., Potapov, P.V., Moore, R., Hancher, M., Turubanova, S.A., Tyukavina, A., Thau, D., Stehman, S.V., Goetz, S.J., Loveland, T.R., Kommareddy, A., Egorov, A., Chini, L., Justice, C.O., Townshend, J.R.G., 2013. High-resolution global maps of 21st-Century forest cover change. Science 342, 850–853. https://doi.org/10.1126/science.1244693.

Harmonized Sentinel-2 MSI: MultiSpectral Instrument, Level-1C (TOA) | Earth engine data catalog, Google for Developers (n.d.). https://developers.google.com/earth-engine/datasets/catalog/COPERNICUS_S2_HARMONIZED (accessed May 1, 2025).

Harrison, G.R., Rigge, M., Assal, T.J., Applestein, C., James, D.K., McCord, S.E., 2025. An accuracy assessment of satellite-derived rangeland fractional cover. Ecol. Indic. 172, 113267. https://doi.org/10.1016/j.ecolind.2025.113267.

Heris, M.P., Bagstad, K.J., Troy, A., O'Neil-Dunne, J., 2022. Assessing the accuracy and potential for improvement of the national land cover database's tree canopy cover dataset in urban areas of the conterminous United States. Remote Sens. 14. https://doi.org/10.3390/rs14051219.

Homer, C., Huang, C., Yang, L., Wylie, B., Coan, M., 2004. Development of a 2001 national land cover database for the United States, photogramm. Eng. Remote Sens. 70, 829–840. https://doi.org/10.14358/PERS.70.7.829.

Homer, C., Dewitz, J., Yang, L., Jin, S., Danielson, P., Xian, G., Coulston, J., Herold, N., Wickham, J., Megown, K., 2015. Completion of the 2011 national land cover database for the conterminous United States – representing a decade of land cover change information. Photogramm. Eng. Rem. Sens. 81, 345–354. https://doi.org/10.1016/S0099-1112(15)30100-2.

I. Housman, Geeviz: a package to help with GEE data processing, analysis, and visualization, (n.d.). https://pypi.org/project/geeviz/.

Housman, I.W., Heyer, J.P., Ruefenacht, B., Schleeweis, K., Megown, K., Bogle, S., Reischmann, J., Ryerson, D., 2025. National Land Cover Database Tree Canopy Cover Methods v2023.5. FSIC-GO-10268-RPT2. U.S. Department of Agriculture, Forest Service, Field Services and Innovation Center- Geospatial Office, Salt Lake City, UT. https://data.fs.usda.gov/geodata/rastergateway/treecanopycover/index.php. (Accessed 9 June 2025).

Huang, C., Yang, L., Wylie, B., Homer, C., 2001. A strategy for estimating tree canopy density using landsat 7 ETM+ and high resolution images over large areas. In: Proceedings of the Third International Conference on Geospatial Information in Agriculture and Forestry, p. 10. Denver, CO. https://pubs.usgs.gov/publication/70231710. (Accessed 1 May 2025).

Jennings, S., Brown, N., Sheil, D., 1999. Assessing forest canopies and understorey illumination: canopy closure, canopy cover and other measures. Forestry 72, 59–74. https://doi.org/10.1093/forestry/72.1.59.

Kennedy, R.E., Yang, Z., Cohen, W.B., 2010. Detecting trends in forest disturbance and recovery using yearly Landsat time series: 1. LandTrendr — temporal segmentation algorithms. Remote Sens. Environ. 114, 2897–2910. https://doi.org/10.1016/j.rse.2010.07.008.

Kennedy, R.E., Andréfouët, S., Cohen, W.B., Gómez, C., Griffiths, P., Hais, M., Healey, S. P., Helmer, E.H., Hostert, P., Lyons, M.B., Meigs, G.W., Pflugmacher, D., Phinn, S.R., Powell, S.L., Scarth, P., Sen, S., Schroeder, T.A., Schneider, A., Sonnenschein, R., Vogelmann, J.E., Wulder, M.A., Zhu, Z., 2014. Bringing an ecological view of change to Landsat-based remote sensing. Front. Ecol. Environ. 12, 339–346. https://doi.org/10.1890/130066.

Kennedy, R.E., Yang, Z., Gorelick, N., Braaten, J., Cavalcante, L., Cohen, W.B., Healey, S., 2018. Implementation of the LandTrendr algorithm on google Earth engine. Remote Sens. 10, 691. https://doi.org/10.3390/rs10050691.

La Puma, I.P., 2023. LANDFIRE Technical Documentation: Open-File Report 2023–1045. U.S. Geological Survey, Reston, VA. https://doi.org/10.3133/ofr20231045.

Landsat Collections in Earth Engine | Earth Engine Data Catalog, Google for developers (n.d.). https://developers.google.com/earth-engine/datasets/catalog/landsat (accessed May 1, 2025).

Lavelle, F.M., Mizzen, D.R., Jackman, A.M., Bausch, D., Vickery, P.J., Rozelle, J., Kelly, M.E., Zuzak, C., 2023. Hurricane wind loss estimation for Puerto Rico and the US Virgin Islands: model implementation and validation. Nat. Hazards Rev. 24, 04023034. https://doi.org/10.1061/NHREFO.NHENG-1638.

Lister, A.J., Andersen, H., Frescino, T., Gatziolis, D., Healey, S., Heath, L.S., Liknes, G.C., McRoberts, R., Moisen, G.G., Nelson, M., Riemann, R., Schleeweis, K., Schroeder, T. A., Westfall, J., Wilson, B.T., 2020. Use of remote sensing data to improve the efficiency of National forest inventories: a case study from the United States National forest inventory. Forests 11, 1364. https://doi.org/10.3390/f11121364.

Ma, Q., Su, Y., Guo, Q., 2017. Comparison of canopy cover estimations from airborne LiDAR, aerial imagery, and satellite imagery. IEEE J. Sel. Top. Appl. Earth Obs 10, 4225–4236. https://doi.org/10.1109/JSTARS.2017.2711482.

Marx, R.W., 1986. The TIGER system: automating the geographic structure of the United States census. Gov. Publ. Rev. 13, 181–201. https://doi.org/10.1016/0277-9390(86)90003-8.

McDonald, R.I., Kroeger, T., Zhang, P., Hamel, P., 2020. The value of US urban tree cover for reducing heat-related health impacts and electricity consumption. Ecosyst 23, 137–150. https://doi.org/10.1007/s10021-019-00395-5.

Millennium Ecosystem Assessment (Program), 2005a. In: Ecosystems and Human well-being: Synthesis. Island Press, Washington, DC.

Millennium Ecosystem Assessment (Program), 2005b. In: Ecosystems and Human well-being: Opportunities and Challenges for Business and Industry. Island Press, Washington, DC. https://www.millenniumassessment.org/documents/document.353.aspx.pdf. (Accessed 29 April 2025).

Mitchell, M.W., 2011. Bias of the random forest Out-of-Bag (OOB) error for certain input parameters. Open J. Stat. 1, 205–211. https://doi.org/10.4236/ojs.2011.13024.

Moisen, G.G., Coulston, J.W., Wilson, B.T., Cohen, W.B., Finco, M.V., 2012. Choosing appropriate subpopulations for modeling tree canopy cover nationwide. In: McWilliams, W., Roesch, F.A. (Eds.), Monitoring Across Borders: 2010 Joint Meeting of the Forest Inventory and Analysis (FIA) Symposium and the Southern Mensurationists, pp. 195–200 e-Gen. Tech. Rep. SRS-157, Asheville, NC. https://research.fs.usda.gov/treesearch/41007. (Accessed 30 April 2025).

Multi-Resolution Land Characteristics Consortium, Data | multi-resolution land characteristics (MRLC) consortium, (n.d.). https://www.mrlc.gov/data (accessed May 1, 2025).

Multi-Resolution Land Characteristics Consortium, MRLC viewer, (n.d.). https://www.mrlc.gov/viewer/(accessed May 1, 2025).

Nelson, M.D., Riitters, K.H., Coulston, J.W., Domke, G.M., Greenfield, E.J., Langner, L.L., Nowak, D.J., O'Dea, C.B., Oswalt, S.N., Reeves, M.C., Wear, D.N., 2020. Defining the United States Land Base: a Technical Document Supporting the USDA Forest Service 2020 RPA Assessment. Gen. Tech. Rep. NRS-191. U.S. Department of Agriculture,

Forest Service, Northern Research Station, Madison, WI. https://research.fs.usda.gov/treesearch/59691. (Accessed 30 April 2025).
Omernik, J.M., Griffith, G.E., 2014. Ecoregions of the conterminous United States: evolution of a hierarchical spatial framework. Environ. Manag. 54, 1249–1266. https://doi.org/10.1007/s00267-014-0364-1.
Oswalt, S.N., Smith, W.B., Miles, P.D., Pugh, S.A., 2019. Forest Resources of the United States, 2017: a Technical Document Supporting the Forest Service 2020 RPA Assessment. Gen. Tech. Rep. WO-97. Department of Agriculture, Forest Service, Washington Office, Washington, DC. https://doi.org/10.2737/WO-GTR-97. (Accessed 30 April 2025).
Pedregosa, F., Varoquaux, G., Gramfort, A., Michel, V., Thirion, B., Grisel, O., Blondel, M., Prettenhofer, P., Weiss, R., Dubourg, V., Vanderplas, J., Passos, A., Cournapeau, D., Brucher, M., Perrot, M., Duchesnay, É., 2011. Scikit-learn: machine learning in python. J. Mach. Learn. Res. 12, 2825–2830. https://doi.org/10.48550/arXiv.1201.0490.
Pestana, S., Lundquist, J.D., 2022. Evaluating GOES-16 ABI surface brightness temperature observation biases over the central Sierra Nevada of California. Remote Sens. Environ. 281, 113221. https://doi.org/10.1016/j.rse.2022.113221.
Pontius Jr., R.G., Francis, Thomas, M., 2025. Millones, A call to interpret disagreement components during classification assessment. Int. J. Geogr. Inf. Sci. 0, 1–18. https://doi.org/10.1080/13658816.2025.2469830.
Potapov, P., Hansen, M.C., Pickens, A., Hernandez-Serna, A., Tyukavina, A., Turubanova, S., Zalles, V., Li, X., Khan, A., Stolle, F., Harris, N., Song, X.-P., Baggett, A., Kommareddy, I., Kommareddy, A., 2022. The global 2000-2020 land cover and land use change dataset derived from the landsat archive: first results, front. Remote Sens. 3. https://doi.org/10.3389/frsen.2022.856903.
Poulos, H.M., Barton, A.M., Koch, G.W., Kolb, T.E., Thode, A.E., 2021. Wildfire severity and vegetation recovery drive post-fire evapotranspiration in a Southwestern pine-oak forest, Arizona, USA. Remote Sens. Ecol. Con. 7, 579–591. https://doi.org/10.1002/rse2.210.
R Core Team, 2020. R: a language and environment for statistical computing. https://www.R-project.org/.
Reams, G.A., Smith, W.D., Hansen, M.H., Bechtold, W.A., Roesch, F.A., Moisen, G.G., 2005. The Forest Inventory and Analysis Sampling Frame. Gen. Tech. Rep. SRS-80. U.S. Department of Agriculture, Forest Service, Southern Research Station, Asheville, NC. https://research.fs.usda.gov/treesearch/20376. (Accessed 1 May 2025).
Riemann, R., Wilson, B.T., Lister, A., Parks, S., 2010. An effective assessment protocol for continuous geospatial datasets of forest characteristics using USFS Forest Inventory and Analysis (FIA) data. Remote Sens. Environ. 114, 2337–2352. https://doi.org/10.1016/j.rse.2010.05.010.
Rittger, K., Raleigh, M.S., Dozier, J., Hill, A.F., Lutz, J.A., Painter, T.H., 2020. Canopy adjustment and improved cloud detection for remotely sensed snow cover mapping. Water Resour. Res. 56, e2019WR024914. https://doi.org/10.1029/2019WR024914.
Ruefenacht, B., Heyer, J., Johnson, V., Goetz, W., Bender, S., Schleeweis, K., Megown, K., 2022. Forest Service Tree Canopy Cover Mapping: 2016 Product Suite and Methods. U.S. Department of Agriculture, Forest Service, Geospatial Technology and Applications Center, Salt Lake City, UT. GTAC-10264-RPT1. https://data.fs.usda.gov/geodata/rastergateway/treecanopycover/docs/TCC_2016_MethodsReport_2022-08-16.pdf.
Sannier, C., Gallego, J., Langanke, T., Donezar, U., Pennec, A., 2023. Tree cover area estimation in Europe based on the combination of in situ reference data and the copernicus high resolution layer on tree cover density. Int. Arch. Photogramm. Remote Sens XLVIII-M-1–2023, 277–284. https://doi.org/10.5194/isprs-archives-XLVIII-M-1-2023-277-2023.
Sexton, J.O., Song, X.-P., Feng, M., Noojipady, P., Anand, A., Huang, C., Kim, D.-H., Collins, K.M., Channan, S., DiMiceli, C., Townshend, J.R., 2013. Global, 30-m resolution continuous fields of tree cover: Landsat-based rescaling of MODIS vegetation continuous fields with lidar-based estimates of error. Int. J. Digit. Earth 6, 427–448. https://doi.org/10.1080/17538947.2013.786146.
Smith, A.M.S., Strand, E.K., Steele, C.M., Hann, D.B., Garrity, S.R., Falkowski, M.J., Evans, J.S., 2008. Production of vegetation spatial-structure maps by per-object analysis of juniper encroachment in multitemporal aerial photographs. Can. J. Rem. Sens. 34, S268–S285. https://doi.org/10.5589/m08-048.
Sohl, T.L., Schleeweis, K., Herold, N., Lang, M.W., Puma, I.P.L., Wickham, J.D., Mueller, R., Rigge, M.B., Dewitz, J., Brown, J.F., Ingebritsen, J., Ellenwood, J., Wengert, E., Rowe, J., Flanagan, P., Kachergis, E., Garthwaite, I., Wu, Z., 2025. An interagency perspective on improving consistency and transparency of land use and land cover mapping. U.S. Geological Survey Circular 1549. U.S. Geological Survey. https://doi.org/10.3133/cir1549.
Stahl, A.T., Andrus, R., Hicke, J.A., Hudak, A.T., Bright, B.C., Meddens, A.J.H., 2023. Automated attribution of forest disturbance types from remote sensing data: a synthesis. Remote Sens. Environ. 285, 113416. https://doi.org/10.1016/j.rse.2022.113416.
Stehman, S.V., Foody, G.M., 2019. Key issues in rigorous accuracy assessment of land cover products. Remote Sens. Environ. 231, 111199. https://doi.org/10.1016/j.rse.2019.05.018.
Su, Y., Weng, K., Lin, C., Zheng, Z., 2021. An improved random forest model for the prediction of dam displacement. IEEE Access 9, 9142–9153. https://doi.org/10.1109/ACCESS.2021.3049578.
Tang, H., Armston, J., Hancock, S., Marselis, S., Goetz, S., Dubayah, R., 2019. Characterizing global forest canopy cover distribution using spaceborne lidar. Remote Sens. Environ. 231, 111262. https://doi.org/10.1016/j.rse.2019.111262.
Tipton, J., Moisen, G., Patterson, P., Jackson, T.A., Coulston, J., 2012. Sampling intensity and normalizations: exploring cost-driving factors in nationwide mapping of tree canopy cover. In: McWilliams, W., Roesch, F.A. (Eds.), Monitoring Across Borders: 2010 Joint Meeting of the Forest Inventory and Analysis (FIA) Symposium and the Southern Mensurationists. e-Gen. Tech. Rep. SRS-157. U.S. Department of Agriculture, Forest Service, Southern Research Station, Asheville, NC, pp. 201–208. https://research.fs.usda.gov/treesearch/41008. (Accessed 30 April 2025).
Tompalski, P., White, J.C., Coops, N.C., Wulder, M.A., Leboeuf, A., Sinclair, I., Butson, C. R., Lemonde, M.-O., 2021. Quantifying the precision of forest stand height and canopy cover estimates derived from air photo interpretation. Forestry 94, 611–629. https://doi.org/10.1093/forestry/cpab022.
USDA farm production and conservation business center geospatial enterprise operations branch, Nat. Agricul. Imagery Program, (n.d.). https://naip-usdaonline.hub.arcgis.com/(accessed May 9, 2025).
USDA Forest Service, Tree canopy cover datasets, (n.d.). https://data.fs.usda.gov/geodata/rastergateway/treecanopycover/.
USDA Forest Service, 2023. USFS landscape change monitoring system conterminous United States version 2024-10. https://data.fs.usda.gov/geodata/rastergateway/LCMS/index.php.
USDA Forest Service, US Geological Survey, Monitoring trends in burn severity thematic burn severity, (n.d.). https://www.mtbs.gov/(accessed May 1, 2025).
USDA Forest Service Geospatial Technology and Applications Center (GTAC), USFS Tree Canopy Cover v2021-4 (CONUS and OCONUS) | Earth Engine Data Catalog, (n.d.). https://developers.google.com/earth-engine/datasets/catalog/USGS_NLCD_RELEASES_2021_REL_TCC_v2021-4 (accessed May 1, 2025).
USDA National Agricultural Statistics Service, 2008. Published crop-specific data layer. https://nassgeodata.gmu.edu/CropScapeUSDA-NASS. (Accessed 30 April 2025).
Vogeler, J.C., Braaten, J.D., Slesak, R.A., Falkowski, M.J., 2018. Extracting the full value of the Landsat archive: Inter-sensor harmonization for the mapping of Minnesota forest canopy cover (1973–2015). Remote Sens. Environ. 209, 363–374. https://doi.org/10.1016/j.rse.2018.02.046.
Vogeler, J.C., Slesak, R.A., Fekety, P.A., Falkowski, M.J., 2020. Characterizing over four decades of Forest disturbance in Minnesota, USA. Forests 11, 362. https://doi.org/10.3390/f11030362.
Vogt, P., Riitters, K., Barredo, J.I., Costanza, J., Eckhardt, B., Schleeweis, K., 2024. Improving forest connectivity assessments using tree cover density maps. Ecol. Indic. 159, 111695. https://doi.org/10.1016/j.ecolind.2024.111695.
Waldner, F., Defourny, P., 2017. Where can pixel counting area estimates meet user-defined accuracy requirements? Int. J. Appl. Earth Obs. Geoinf. 60, 1–10. https://doi.org/10.1016/j.jag.2017.03.014.
White, J.C., Wulder, M.A., Hermosilla, T., Coops, N.C., Hobart, G.W., 2017. A nationwide annual characterization of 25 years of forest disturbance and recovery for Canada using Landsat time series. Remote Sens. Environ. 194, 303–321. https://doi.org/10.1016/j.rse.2017.03.035.
Wickham, J., Homer, C., Vogelmann, J., McKerrow, A., Mueller, R., Herold, N., Coulston, J., 2014. The multi-resolution land characteristics (MRLC) consortium — 20 years of development and integration of USA national land cover data. Remote Sens. 6, 7424–7441. https://doi.org/10.3390/rs6087424.
Wickham, J., Neale, A., Riitters, K., Nash, M., Dewitz, J., Jin, S., van Fossen, M., Rosenbaum, D., 2023. Where forest may not return in the Western United States. Ecol. Indic. 146, 109756. https://doi.org/10.1016/j.ecolind.2022.109756.
Woodcock, C.E., Allen, R., Anderson, M., Belward, A., Bindschadler, R., Cohen, W., Gao, F., Goward, S.N., Helder, D., Helmer, E., Nemani, R., Oreopoulos, L., Schott, J., Thenkabail, P.S., Vermote, E.F., Vogelmann, J., Wulder, M.A., Wynne, R., 2008. Free access to landsat imagery. Science 320. https://doi.org/10.1126/science.320.5879.1011a, 1011–1011.
Woodcock, C.E., Loveland, T.R., Herold, M., Bauer, M.E., 2020. Transitioning from change detection to monitoring with remote sensing: a paradigm shift. Remote Sens. Environ. 238, 111558. https://doi.org/10.1016/j.rse.2019.111558.
Wu, X., Xiao, L., Sun, Y., Zhang, J., Ma, T., He, L., 2022. A survey of human-in-the-loop for machine learning. Future Gener. Comput. Syst. 135, 364–381. https://doi.org/10.1016/j.future.2022.05.014.
Wulder, M.A., Masek, J.G., Cohen, W.B., Loveland, T.R., Woodcock, C.E., 2012. Opening the archive: how free data has enabled the science and monitoring promise of Landsat. Remote Sens. Environ. 122, 2–10. https://doi.org/10.1016/j.rse.2012.01.010.
Wulder, M.A., Roy, D.P., Radeloff, V.C., Loveland, T.R., Anderson, M.C., Johnson, D.M., Healey, S., Zhu, Z., Scambos, T.A., Pahlevan, N., Hansen, M., Gorelick, N., Crawford, C.J., Masek, J.G., Hermosilla, T., White, J.C., Belward, A.S., Schaaf, C., Woodcock, C.E., Huntington, J.L., Lymburner, L., Hostert, P., Gao, F., Lyapustin, A., Pekel, J.-F., Strobl, P., Cook, B.D., 2022. Fifty years of Landsat science and impacts. Remote Sens. Environ. 280, 113195. https://doi.org/10.1016/j.rse.2022.113195.
Yang, L., Jin, S., Danielson, P., Homer, C., Gass, L., Bender, S.M., Case, A., Costello, C., Dewitz, J., Fry, J., Funk, M., Granneman, B., Liknes, G.C., Rigge, M., Xian, G., 2018. A new generation of the United States National land cover database: requirements, research priorities, design, and implementation strategies. ISPRS J. Photogrammetry Remote Sens. 146, 108–123. https://doi.org/10.1016/j.isprsjprs.2018.09.006.
Zalles, V., Harris, N., Stolle, F., Hansen, M.C., 2024. Forest definitions require a re-think. Commun. Earth Environ. 5, 1–4. https://doi.org/10.1038/s43247-024-01779-9.
Zanaga, D., Van De Kerchove, R., Daems, D., De Keersmaecker, W., Brockmann, C., Kirches, G., Wevers, J., Cartus, O., Santoro, M., Fritz, S., Lesiv, M., Herold, M., Tsendbazar, N.E., Xu, P., Ramoino, F., Arino, O., 2022. ESA WorldCover 10 m 2021 v200. https://doi.org/10.5281/zenodo.7254221.
Zhao, F., Huang, C., Goward, S.N., Schleeweis, K., Rishmawi, K., Lindsey, M.A., Denning, E., Keddell, L., Cohen, W.B., Yang, Z., Dungan, J.L., Michaelis, A., 2018. Development of Landsat-based annual US forest disturbance history maps (1986–2010) in support of the North American Carbon Program (NACP). Remote Sens. Environ. 209, 312–326. https://doi.org/10.1016/j.rse.2018.02.035.